Inner and outer approximation of the image of a set by a nonlinear function [1]

Maël Godard

Lab-STICC, ROBEX Team, ENSTA, 2 rue François Verny, Brest, 29200, France

Luc Jaulin

Lab-STICC, ROBEX Team, ENSTA, 2 rue François Verny, Brest, 29200, France

Damien Massé

Lab-STICC, ROBEX Team, Université de Bretagne Occidentale, 20 avenue Le Gorgeu, Brest, 29200, France

Abstract

This paper proposes an original method to compute an inner and an outer approximation of the image $\mathbf{f}(\mathbb{X})$ of a subset $\mathbb{X}$ of $\mathbb{R}^n$ (*e.g.*, $\mathbb{X}$ is the unit ball) by a smooth nonlinear function $\mathbf{f} : \mathbb{R}^n \to \mathbb{R}^n$. A boundary approach is proposed. More precisely, the boundary $\partial\mathbf{f}(\mathbb{X})$ will be covered by parallelepipeds in order to get an accurate enclosure of $\mathbf{f}(\mathbb{X})$.

Keywords: Parallelepipeds, Boundary approach, Inclusion function, Gnomonic atlas

1. Introduction

Several approaches are used to represent and propagate uncertainties. The most popular representations are probability distributions [1], belief functions (see e.g. [2, 3]), possibility distributions [4] and sets [5, 6]. Each representation has developed its own tools to propagate the uncertainties through a constraint network. Without any doubt, the most ubiquitous propagation tool is the Bayesian filter which can be declined into the Kalman filter

[1] This work was supported by the Defense Innovation Agency (AID) and the Brittany Region.

[7] for linear systems and the particle filter [8] for nonlinear systems.

For the propagation steps and for any of the approaches, the two basic problems that have to be solved are the *inverse problem* [9] and *the direct problem* [1, 10]. To define them, we consider two vectors $\mathbf{x}$ and $\mathbf{y}$ linked by the constraint $\mathbf{y} = \mathbf{f}(\mathbf{x})$, where $\mathbf{f} : \mathbb{R}^m \mapsto \mathbb{R}^n$.

- The *direct problem*: Assume that $\mathbf{x}$ is known with some uncertainty, estimate $\mathbf{y} \in \mathbb{R}^n$ and characterize the uncertainty for $\mathbf{y}$.
- The *inverse problem*: Assume that $\mathbf{y}$ is known with some uncertainty, estimate $\mathbf{x} \in \mathbb{R}^m$ and characterize the uncertainty for $\mathbf{x}$.

In this paper, we will focus on the direct problem. In a probability framework, one of the most famous results is obtained [11] when $\mathbf{f}$ is affine (*i.e.*, $\mathbf{f}(\mathbf{x}) = \mathbf{A}\mathbf{x} + \mathbf{b}$) and $\mathbf{x}$ is Gaussian $(\bar{\mathbf{x}}, \mathbf{\Gamma_x})$. In such a case, Kolmogorov has shown that $\mathbf{y}$ is also Gaussian $(\bar{\mathbf{y}}, \mathbf{\Gamma_y})$ with $\bar{\mathbf{y}} = \mathbf{A}\bar{\mathbf{x}} + \mathbf{b}$ and $\mathbf{\Gamma_y} = \mathbf{A}\mathbf{\Gamma_x}\mathbf{A}^{\mathrm{T}}$. Now, this specific case is an exception and solving the direct problem in a reliable way can be considered as open in the general case, for all types of uncertainty representation.

In a set-membership framework, *i.e.*, $\mathbf{x}$ is known to belong to a set $\mathbb{X}$, then, the uncertainty for $\mathbf{y}$ is represented by the set $\mathbb{Y} = \mathbf{f}(\mathbb{X})$. Interval methods [12, 13] can used to compute such an outer enclosure for $\mathbb{Y}$, but the pessimism is often too large. Other types of sets such as zonotopes [14] or ellipsoids [15, 16] have been considered to limit the pessimism, but again, the pessimism still exists and cannot be quantified. The control of the overestimation can only be reached if bisections are performed which makes the direct problem intractable [17], even if $\mathbf{f}$ is affine [18]. Some efficient algorithms have been proposed to find an outer enclosure for $\mathbb{Y}$ (see *e.g.*, [19]), but to our knowledge, no algorithm has been proposed to find an inner approximation.

In this paper, we propose an original approach to characterize a set defined as the image of a set $\mathbb{X} \subset \mathbb{R}^n$ (a ball for instance) by nonlinear function $\mathbf{f} : \mathbb{R}^n \to \mathbb{R}^n$. Our approach proposes to cover $\partial\mathbf{f}(\mathbb{X})$, the boundary of $\mathbf{f}(\mathbb{X})$, as proposed in [20] where the covering was made with boxes. Here, we propose a covering with small parallelepipeds instead which creates some interesting connections with the literature on geometric inference. Indeed, the use of parallelepipeds also allows us to represent the set $\mathbb{Y} = \mathbf{f}(\mathbb{X})$ using a Delaunay triangulation [21, 22].

Our main contribution is to propose an approximation which is less conservative (in term of convergence order) and which provides both an inner and an outer approximation of the image set $\mathbb{Y}$.

The paper is organized as follows. Section 2 explains how to get an accurate parallelepiped outer approximation of the image of a small box through a nonlinear function $\mathbf{f}$. Section 3 provides theoretical results to show that the parallelepiped approximation has an order greater than existing interval methods, in the case where $\mathbf{f} : \mathbb{R}^m \to \mathbb{R}^n$ with $m < n$. Section 4 introduces the concept of gnomonic atlas to cover the boundary of $\mathbb{X}$ [23]. This covering will allow us to focus on the image of the boundary in order be more accurate. Section 5 illustrates on some examples how our boundary parallelepiped approach can be used to compute the inner and outer approximations of $\mathbb{Y}$. Section 6 concludes the paper.

Notations

In this paper, we will use the following notations

- Vectors $\mathbf{x} \in \mathbb{R}^n$ are written in bold.
- The norm $\|\mathbf{x}\|$ of a vector $\mathbf{x}$ always means the Euclidean norm.
- The upper bound of an interval $[a]$ is denoted by $\mathrm{ub}([a])$ and its lower bound by $\mathrm{lb}([a])$.
- A box $[\mathbf{x}]$ of $\mathbb{R}^n$ is the Cartesian product of n intervals:
  $[\mathbf{x}] = \{\mathbf{x} \in \mathbb{R}^n \mid a_i \leq x_i \leq b_i \text{ for } i = 1, \cdots, n\}$
  where $a_i \in \mathbb{R}$, $b_i \in \mathbb{R}$.
- The width $w([\mathbf{x}])$ of a box $[\mathbf{x}] \subset \mathbb{R}^n$ is the length of its largest side:
  $w([\mathbf{x}]) = \max_{i \in \{1,\ldots,n\}} \mathrm{ub}([x_i]) - \mathrm{lb}([x_i])$.
- The center of a box $[\mathbf{x}]$ is denoted by $\bar{\mathbf{x}}$.
- Parallelepipeds are written with angles, for example $\langle \mathbf{x} \rangle$. They will be defined in Section 2.1.
- The set of boxes of $\mathbb{R}^n$ is denoted by $\mathbb{IR}^n$. The set of parallelepipeds of $\mathbb{R}^n$ is denoted by $\mathbb{PR}^n$.
- The m dimensional unit ball is $\mathbb{U} = \{\mathbf{u} \in \mathbb{R}^m | \|\mathbf{u}\| \leq 1\}$.

- The notion of boundary which is considered in this paper is the *topological boundary*.
- The boundary of a set $\mathbb{X}$ is denoted by $\partial\mathbb{X}$.

2. Parallelepiped approximation

In this section, we show how to compute an accurate approximation of $\mathbf{f}([\mathbf{x}])$, when $[\mathbf{x}]$ is a tiny box (*i.e.*, sufficiently small) and $\mathbf{f} : \mathbb{R}^m \to \mathbb{R}^n$. We consider the more general case where $m \leq n$ (instead of $m = n$ given in the introduction). The reason for this is that the case $m < n$ will be needed later to compute the image of $\partial\mathbb{X}$ the boundary of the set of interest $\mathbb{X}$.

2.1. Parallelepiped inclusion function

A *parallelepiped* is a subset of $\mathbb{R}^n$ of the form

$$\langle \mathbf{y} \rangle = \bar{\mathbf{y}} + \mathbf{A} \cdot [-1, 1]^m = \{\bar{\mathbf{y}} + \mathbf{A} \cdot \mathbf{x} \,|\, \mathbf{x} \in [-1, 1]^m\} \tag{1}$$

where $m \leq n$.

When $m > n$, $\langle \mathbf{y} \rangle$ is a zonotope [14, 24] (not used in this paper as $m \leq n$). The matrix $\mathbf{A}$ is called the *shape matrix*. Its columns are called the *support vectors* of $\langle \mathbf{y} \rangle$. This matrix $\mathbf{A}$ can be uniquely decomposed into a matrix $\mathbf{N}$ and a matrix $\mathbf{D}$ such that

- The columns of $\mathbf{N}$ have unit length
- the matrix $\mathbf{D}$ is diagonal and positive
- $\mathbf{A} = \mathbf{N} \cdot \mathbf{D}$

The matrix $\mathbf{N}$ will be called the *normalized matrix*. For the remaining of this article the notion of *decomposition of a matrix* will refer to this unique decomposition.

Parallelepipeds are efficient wrappers to enclose a set [25, 26]. Consider a function $\mathbf{f} : \mathbb{R}^m \to \mathbb{R}^n$, $m < n$, a *parallelepiped inclusion function* is a function

$$\langle \mathbf{f} \rangle : \begin{array}{ccc} \mathbb{IR}^m & \to & \mathbb{PR}^n \\ [\mathbf{x}] & \mapsto & \langle \mathbf{f} \rangle([\mathbf{x}]) \end{array} \tag{2}$$

such that

$$\mathbf{f}([\mathbf{x}]) \subset \langle \mathbf{f} \rangle([\mathbf{x}]). \tag{3}$$

This definition is illustrated by Figure 1 in the case where $m = 1$ and $n = 2$. In the figure, the graph of $\mathbf{f}$ given by $\{(\mathbf{x}, \mathbf{f}(\mathbf{x})), \mathbf{x} \in \mathbb{R}^m\}$ is painted black. Two projections of the graph are given (gray). One of the projection corresponds to the image of $\mathbf{f}$: $\mathbf{f}(\mathbb{R}^m) = \{\mathbf{f}(\mathbf{x}), \mathbf{x} \in \mathbb{R}^m\}$. The blue segment of $\mathbb{R}^n$ corresponds to the image of $[\mathbf{x}]$ by $\mathbf{f}$. It is this blue segment which is enclosed in the parallelepiped $\langle \mathbf{f} \rangle([\mathbf{x}])$.

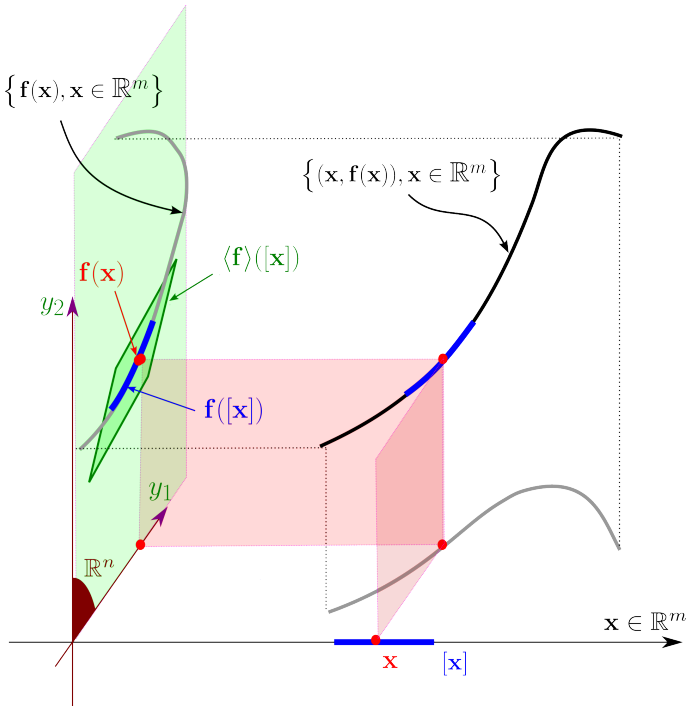

Figure 1: Parallelepiped inclusion function $\langle \mathbf{f} \rangle$

2.2. Approximation theorem

To get a parallelepiped inclusion function for $\mathbf{f} : \mathbb{R}^m \mapsto \mathbb{R}^n$, we need to compute a parallelepiped which encloses $\mathbf{f}([\mathbf{x}])$, for a given box $[\mathbf{x}]$ of $\mathbb{R}^m$.

Definition 1. Consider two intervals $[x]$ and $[y]$. Their product is defined in [6] as

$$[x] \cdot [y] = \{x \cdot y \in \mathbb{R} \mid x \in [x]\,,\ y \in [y]\} \tag{4}$$

Remark 1. By relying on Definition 1, operations like the product of two matrices or a matrix and a vector can be extended to interval matrices and interval vectors.

Theorem 1. *Consider a function* $\mathbf{f}$ *of class* C^1 *(*i.e.*, differentiable with its derivative continuous) from* $\mathbb{R}^m$ *to* $\mathbb{R}^n$ *and a box* $[\mathbf{x}] \in \mathbb{IR}^m$ *with center* $\bar{\mathbf{x}}$*. Define the linear approximation*

$$\boldsymbol{\ell}(\mathbf{x}) = \mathbf{f}(\bar{\mathbf{x}}) + \frac{d\mathbf{f}}{d\mathbf{x}}(\bar{\mathbf{x}}) \cdot (\mathbf{x} - \bar{\mathbf{x}}) \tag{5}$$

as illustrated by Figure 2. We have

$$\forall \mathbf{x} \in [\mathbf{x}], \|\mathbf{f}(\mathbf{x}) - \boldsymbol{\ell}(\mathbf{x})\| \leq \rho \tag{6}$$

where

$$\rho = \rho_{\mathbf{f}}([\mathbf{x}]) = ub\left(\left\|\left(\left[\frac{d\mathbf{f}}{d\mathbf{x}}\right]([\mathbf{x}]) - \frac{d\mathbf{f}}{d\mathbf{x}}(\bar{\mathbf{x}})\right) \cdot ([\mathbf{x}] - \bar{\mathbf{x}})\right\|\right) \tag{7}$$

Moreover

$$\rho = o(w([\mathbf{x}])), \tag{8}$$

i.e., ρ *is small compared to* $\varepsilon = w([\mathbf{x}])$*, when* $w([\mathbf{x}])$ *is small.*

Remark 2. In Equation 7, $\left[\frac{d\mathbf{f}}{d\mathbf{x}}\right]$ is an inclusion function of $\frac{d\mathbf{f}}{d\mathbf{x}}$ in the sense of Moore [12]. This means that $\left[\frac{d\mathbf{f}}{d\mathbf{x}}\right]([\mathbf{x}])$ contains all $\frac{d\mathbf{f}}{d\mathbf{x}}(\mathbf{x})$, for $\mathbf{x} \in [\mathbf{x}]$. Thus $\left[\frac{d\mathbf{f}}{d\mathbf{x}}\right]([\mathbf{x}])$ is an interval matrix. Since $[\mathbf{x}]$ is an interval vector (or a box), the quantity $[\mathbf{a}] = \left(\left[\frac{d\mathbf{f}}{d\mathbf{x}}\right]([\mathbf{x}]) - \frac{d\mathbf{f}}{d\mathbf{x}}(\bar{\mathbf{x}})\right) \cdot ([\mathbf{x}] - \bar{\mathbf{x}})$ can be computed as suggested by Remark 1 and is also an interval vector. The norm in (7), $\|[\mathbf{a}]\|$ has also to be understood in the Moore's sense, *i.e.*, $\|[\mathbf{a}]\| = \{n \in \mathbb{R} | \exists \mathbf{a} \in [\mathbf{a}], n = \|\mathbf{a}\|\}$. Therefore $\|[\mathbf{a}]\|$ is an interval from which we extract the upper bound.

Proof. Let us bound the error

$$\begin{array}{rcl} \mathbf{e} & = & \mathbf{f}(\mathbf{x}) - \boldsymbol{\ell}(\mathbf{x}) \\ & = & \mathbf{f}(\mathbf{x}) - \mathbf{f}(\bar{\mathbf{x}}) - \frac{d\mathbf{f}}{d\mathbf{x}}(\bar{\mathbf{x}}) \cdot (\mathbf{x} - \bar{\mathbf{x}}) \end{array} \tag{9}$$

using the methodology given is [27], Section 4.3, based on the centered form [12]. Since $\mathbf{x} \in [\mathbf{x}]$, we get

$$\begin{array}{rcl} \mathbf{e}(\mathbf{x}) & \in & [\mathbf{e}_c]([\mathbf{x}]) \\ & = & \underbrace{\mathbf{e}(\bar{\mathbf{x}})}_{=\mathbf{0}} + \left[\frac{d\mathbf{e}}{d\mathbf{x}}\right]([\mathbf{x}]) \cdot ([\mathbf{x}] - \bar{\mathbf{x}}) \\ & = & \left[\frac{d(\mathbf{f}(\mathbf{x}) - \boldsymbol{\ell}(\mathbf{x}))}{d\mathbf{x}}\right]([\mathbf{x}]) \cdot ([\mathbf{x}] - \bar{\mathbf{x}}) \\ & = & \left(\left[\frac{d\mathbf{f}}{d\mathbf{x}}\right]([\mathbf{x}]) - \frac{d\mathbf{f}}{d\mathbf{x}}(\bar{\mathbf{x}})\right) \cdot ([\mathbf{x}] - \bar{\mathbf{x}}) \end{array} \tag{10}$$

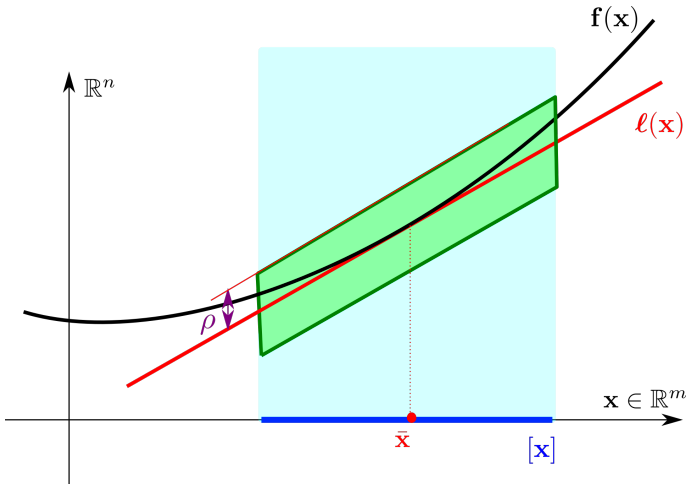

Figure 2: Principle of the parallelepiped enclosure

The smallest ball which encloses the box $[\mathbf{e}_c]([\mathbf{x}])$ has a radius $\rho = \text{ub}(\|[\mathbf{e}_c]([\mathbf{x}])\|)$. Since

$$\begin{array}{rcl} w\left(\left[\frac{d\mathbf{f}}{d\mathbf{x}}\right]([\mathbf{x}]) - \frac{d\mathbf{f}}{d\mathbf{x}}(\bar{\mathbf{x}})\right) & = & O(w([\mathbf{x}])) \\ w([\mathbf{x}] - \bar{\mathbf{x}}) & = & O(w([\mathbf{x}])) \end{array} \tag{11}$$

we have $w([\mathbf{e}_c]) = o(w([\mathbf{x}]))$. Moreover, since $\mathbf{0} \in [\mathbf{e}_c]$, we get $\text{ub}([\mathbf{e}_c]) = o(w([\mathbf{x}]))$, *i.e.*, $\rho = o(w([\mathbf{x}]))$. □

Definition 2. The *Hausdorff distance* expresses how far two compact subsets of a metric space are. Let $(\mathbb{M}, d)$ be a metric space and $\mathbb{A} \subset \mathbb{M}$ and $\mathbb{B} \subset \mathbb{M}$ be two non-empty compact subsets of $\mathbb{M}$. The *Hausdorff distance* between $\mathbb{A}$ and $\mathbb{B}$ is defined by :

$$h(\mathbb{A}, \mathbb{B}) = \max\left\{\sup_{a\in\mathbb{A}} d(a, \mathbb{B}), \sup_{b\in\mathbb{B}} d(b, \mathbb{A})\right\} \tag{12}$$

Where $d(a, \mathbb{B}) = \inf_{b\in\mathbb{B}} d(a, b)$ and $d(b, \mathbb{A}) = \inf_{a\in\mathbb{A}} d(b, a)$.

Corollary 1. *Given a C^1 function $\mathbf{f}$ from $\mathbb{R}^m$ to $\mathbb{R}^n$ and a box $[\mathbf{x}] \in \mathbb{IR}^m$. We have*

$$\mathbf{f}([\mathbf{x}]) \subset \boldsymbol{\ell}([\mathbf{x}]) + \rho\mathbb{U} \tag{13}$$

where $\mathbb{U}$ is the unit ball of $\mathbb{R}^n$, $\rho = \rho_{\mathbf{f}}([\mathbf{x}])$ (see (7)) and $\boldsymbol{\ell}([\mathbf{x}])$ is defined by (5). Moreover, the Hausdorff distance $h(\mathbf{f}([\mathbf{x}]), \boldsymbol{\ell}([\mathbf{x}]))$ between $\mathbf{f}([\mathbf{x}])$ and its approximation $\boldsymbol{\ell}([\mathbf{x}])$ is $o(w([\mathbf{x}]))$.

Proof. The inclusion is a consequence of Theorem 1. Moreover

$$\begin{array}{rcl} h(\mathbf{f}([\mathbf{x}]), \boldsymbol{\ell}([\mathbf{x}])) & \leq & \rho \text{ see (6)} \\ & = & \text{ub}\left(\left\|\left(\left[\frac{d\mathbf{f}}{d\mathbf{x}}\right]([\mathbf{x}]) - \frac{d\mathbf{f}}{d\mathbf{x}}(\bar{\mathbf{x}})\right) \cdot ([\mathbf{x}] - \bar{\mathbf{x}})\right\|\right) \\ & = & O\left\|\left(\left[\frac{d\mathbf{f}}{d\mathbf{x}}\right]([\mathbf{x}]) - \frac{d\mathbf{f}}{d\mathbf{x}}(\bar{\mathbf{x}})\right) \cdot ([\mathbf{x}] - \bar{\mathbf{x}})\right\| \\ & = & O\left\|\left(\left[\frac{d\mathbf{f}}{d\mathbf{x}}\right]([\mathbf{x}]) - \frac{d\mathbf{f}}{d\mathbf{x}}(\bar{\mathbf{x}})\right)\right\| \cdot O\left\|([\mathbf{x}] - \bar{\mathbf{x}})\right\| \\ & = & O\left\|w([\mathbf{x}])\right\| \cdot O\left\|w([\mathbf{x}])\right\| \\ & = & o(w([\mathbf{x}])) \end{array} \tag{14}$$

□

2.3. Parallelepiped inflation

Corollary 1 provides a linear approximation $\boldsymbol{\ell}([\mathbf{x}])$ for the set $\mathbf{f}([\mathbf{x}])$ to be approximated. The set $\boldsymbol{\ell}([\mathbf{x}])$ is a flat parallelepiped which has the form

$$\boldsymbol{\ell}([\mathbf{x}]) = \{\mathbf{y} \in \mathbb{R}^n | \exists \mathbf{x} \in [-1,1]^m, \mathbf{y} = \mathbf{A}\mathbf{x} + \mathbf{b}\}. \tag{15}$$

In this section, we show how to inflate $\boldsymbol{\ell}([\mathbf{x}])$ to obtain a parallelepiped $\langle \mathbf{z} \rangle \in \mathbb{PR}^n$ which encloses the set $\boldsymbol{\ell}([\mathbf{x}]) + \rho\mathbb{U}$. The principle can be found in [28].

2.3.1. Principle

Definition 3. The two parallelepipeds of $\mathbb{PR}^n$

$$\begin{array}{rcl} \langle \mathbf{y} \rangle & = & \bar{\mathbf{y}} + \mathbf{A} \cdot [-1,1]^m \\ \langle \mathbf{z} \rangle & = & \bar{\mathbf{z}} + \mathbf{B} \cdot [-1,1]^m \end{array} \tag{16}$$

have similar shapes iff

$$\mathbf{A} = \mathbf{B} \cdot \mathbf{D} \cdot \mathbf{P} \tag{17}$$

where $\mathbf{D}$ is a diagonal matrix and $\mathbf{P}$ is a permutation matrix. This means that two parallelepipeds have the same shape iff the transformation between them is a rescaling and eventually a rearrangement of their generators.

Remark 3. In particular, if the decomposition described in Section 2.1 of $\mathbf{A}$ and $\mathbf{B}$ gives $\mathbf{A} = \mathbf{N} \cdot \mathbf{D}_1$ and $\mathbf{B} = \mathbf{N} \cdot \mathbf{D}_2$, they have the same shape. In addition, the transformation between $\mathbf{A}$ and $\mathbf{B}$ is a pure rescaling without permutation. Indeed, as the matrices $\mathbf{D}_1$ and $\mathbf{D}_2$ are diagonal, they are invertible. Then

$$\begin{array}{rcl} \mathbf{A} & = & \mathbf{N} \cdot \mathbf{D}_1 \\ & = & \mathbf{N} \cdot \mathbf{D}_2 \cdot \mathbf{D}_2^{-1} \cdot \mathbf{D}_1 \\ & = & \mathbf{B} \cdot \mathbf{D}_2^{-1} \cdot \mathbf{D}_1 \end{array}$$

Then Equation 17 is verified with $\mathbf{D} = \mathbf{D}_2^{-1} \cdot \mathbf{D}_1$ and $\mathbf{P}$ is the identity.

Proposition 1. *The Minkowski sum of* $\langle \mathbf{y} \rangle = \bar{\mathbf{y}} + \mathbf{A} \cdot [-1,1]^m$ *and* $\langle \mathbf{z} \rangle = \bar{\mathbf{z}} + \mathbf{B} \cdot [-1,1]^m$ *is*

$$\langle \mathbf{y} \rangle + \langle \mathbf{z} \rangle = (\bar{\mathbf{y}} + \bar{\mathbf{z}}) + (\mathbf{A} + \mathbf{B}) \cdot [-1,1]^m \tag{18}$$

if the decomposition of $\mathbf{A}$ *and* $\mathbf{B}$ *gives the same normalized matrix.*

Proof. As explained in Remark 3, the ith column $\mathbf{b}_i$ of $\mathbf{B}$ is related to the ith column $\mathbf{a}_i$ of $\mathbf{A}$ by the relation

$$\mathbf{b}_i = d_i \mathbf{a}_i \tag{19}$$

where d_i is the *ith* entry of the diagonal matrix $\mathbf{D}$. Thus

$$\begin{aligned}
\langle \mathbf{y} \rangle + \langle \mathbf{z} \rangle &= \{\bar{\mathbf{y}} + \mathbf{A} \cdot \mathbf{x} \,|\, \mathbf{x} \in [-1,1]^m\} + \{\bar{\mathbf{z}} + \mathbf{B} \cdot \mathbf{r} \,|\, \mathbf{r} \in [-1,1]^m\} \\
&= \bar{\mathbf{y}} + \mathbf{a}_1 \cdot [-1,1] + \cdots + \mathbf{a}_m \cdot [-1,1] + \bar{\mathbf{z}} + \mathbf{b}_1 \cdot [-1,1] + \cdots + \mathbf{b}_m \cdot [-1,1] \\
&= \bar{\mathbf{y}} + \bar{\mathbf{z}} + \mathbf{a}_1 \cdot [-1,1] + \mathbf{b}_1 \cdot [-1,1] + \cdots + \mathbf{a}_m \cdot [-1,1] + \mathbf{b}_m \cdot [-1,1] \\
&= \bar{\mathbf{y}} + \bar{\mathbf{z}} + \mathbf{a}_1 \cdot [-1,1] + d_1 \mathbf{a}_1 \cdot [-1,1] + \cdots + \mathbf{a}_m \cdot [-1,1] + d_m \mathbf{a}_m \cdot [-1,1] \\
&= \bar{\mathbf{y}} + \bar{\mathbf{z}} + \mathbf{a}_1 \cdot (1 + d_1) \cdot [-1,1] + \cdots + \mathbf{a}_m \cdot (1 + d_m) \cdot [-1,1] \text{ (since } d_i > 0) \\
&= \bar{\mathbf{y}} + \bar{\mathbf{z}} + (\mathbf{a}_1 + d_1 \mathbf{a}_1) \cdot [-1,1] + \cdots + (\mathbf{a}_m + d_m \mathbf{a}_m) \cdot [-1,1] \\
&= \bar{\mathbf{y}} + \bar{\mathbf{z}} + (\mathbf{a}_1 + \mathbf{b}_1) \cdot [-1,1] + \cdots + (\mathbf{a}_m + \mathbf{b}_m) \cdot [-1,1]) \\
&= \{\bar{\mathbf{y}} + \bar{\mathbf{z}} + (\mathbf{A} + \mathbf{B}) \cdot \mathbf{x} \,|\, \mathbf{x} \in [-1,1]^m\}
\end{aligned}$$

□

Illustration. Assume that we want to enclose the Minkowski sum $\langle \mathbf{y} \rangle + \mathbb{U}$ of a parallelepiped $\langle \mathbf{y} \rangle$ and a disk $\mathbb{U}$. We first enclose $\mathbb{U}$ inside a parallelepiped $\langle \mathbf{e} \rangle$ the shape of which is similar to $\langle \mathbf{y} \rangle$. Then, we compute $\langle \mathbf{y} \rangle + \langle \mathbf{e} \rangle$. This is illustrated by Figure 3.

This principle will now be used to inflate the flat parallelepiped (which corresponds to $\boldsymbol{\ell}([\mathbf{x}])$):

$$\langle \mathbf{y} \rangle = \{\mathbf{y} \in \mathbb{R}^n | \exists \mathbf{x} \in [-1,1]^m, \mathbf{y} = \mathbf{A}\mathbf{x} + \mathbf{b}\}. \tag{20}$$

As a consequence we will be able to compute a parallelepiped $\langle \mathbf{z} \rangle$ which contains $\mathbf{f}([\mathbf{x}])$.

2.3.2. Centered inflation, square case

We assume here that $m = n$.

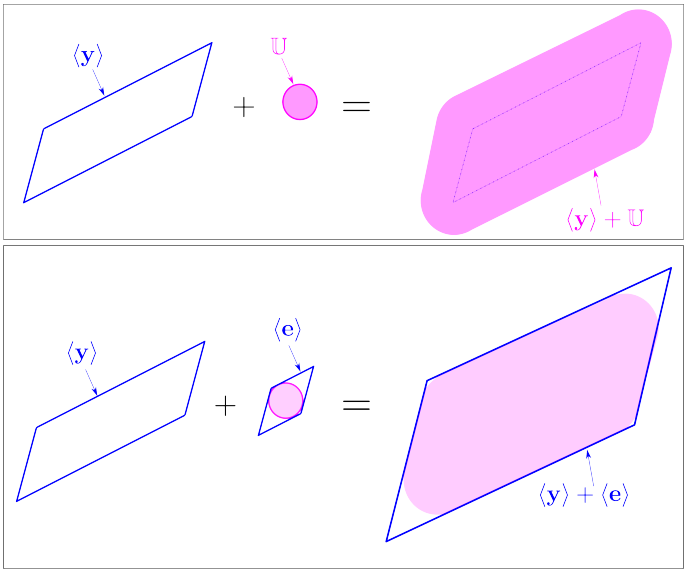

Figure 3: Inflation of a parallelepiped $\langle \mathbf{y} \rangle$ by a disk $\mathbb{U}$. Both $\langle \mathbf{y} \rangle$ and $\langle \mathbf{e} \rangle$ have a similar shape

Proposition 2. *Define the m dimensional centered parallelepiped*

$$\langle \mathbf{y} \rangle = \mathbf{A} \cdot \begin{pmatrix} [-e_1, e_1] \\ \vdots \\ [-e_m, e_m] \end{pmatrix} \tag{21}$$

where $\mathbf{A}$ is an invertible square matrix. Consider the m dimensional unit ball $\mathbb{U}$ and an inflation coefficient $\rho > 0$. The parallelepiped

$$\langle \mathbf{z} \rangle = \mathbf{A} \cdot \begin{pmatrix} e_1 + \rho\sqrt{q_1} & 0 & \cdots & 0 \\ 0 & e_2 + \rho\sqrt{q_2} & & \vdots \\ \vdots & & \ddots & 0 \\ 0 & \cdots & 0 & e_m + \rho\sqrt{q_m} \end{pmatrix} \cdot [-1, 1]^m, \tag{22}$$

where the q_i is the ith diagonal element of the matrix $\mathbf{Q} = \left(\mathbf{A}^T\mathbf{A}\right)^{-1}$, satisfies

$$\langle \mathbf{z} \rangle \supset \langle \mathbf{y} \rangle + \rho\mathbb{U}. \tag{23}$$

Figure 4 illustrates the inflation in the plane supported by $\mathbf{a}_1 = (5, 0)$, $\mathbf{a}_2 = (5, 2)$, the columns of $\mathbf{A}$ and $\rho = 1$.

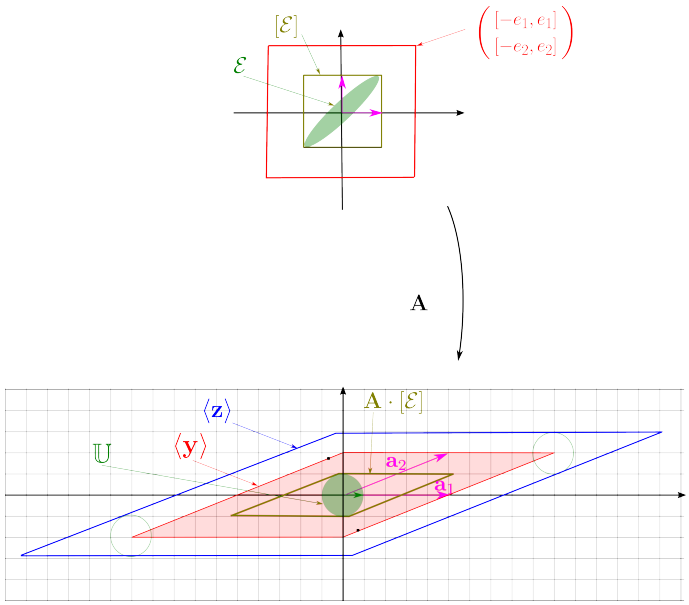

Figure 4: Inflation of a parallelepiped in the case $m = n = 2$

Proof. We want to find a parallelepiped which encloses $\langle \mathbf{y} \rangle + \rho\mathbb{U}$. For this, we need to find a parallelepiped with a shape similar to $\langle \mathbf{y} \rangle$ which encloses the ball $\mathbb{U}$. Since $\mathbf{A}$ is invertible, we have

$$\mathbb{U} = \mathbf{A} \cdot \mathcal{E} \tag{24}$$

where $\mathcal{E}$ is the ellipsoid given by

$$\mathcal{E} = \left\{ \mathbf{x} \in \mathbb{R}^m | \mathbf{x}^{\mathrm{T}} \mathbf{A}^{\mathrm{T}} \mathbf{A} \mathbf{x} \leq 1 \right\}. \tag{25}$$

The smallest box with respect to the inclusion which encloses $\mathcal{E}$ is [16]

$$[\mathcal{E}] = \begin{pmatrix} \sqrt{q_1} & 0 & \cdots & 0 \\ 0 & \sqrt{q_2} & & \vdots \\ \vdots & & \ddots & 0 \\ 0 & \cdots & 0 & \sqrt{q_m} \end{pmatrix} \cdot \begin{pmatrix} [-1,1] \\ \vdots \\ [-1,1] \end{pmatrix} \tag{26}$$

Since

$$\begin{aligned}\langle \mathbf{y} \rangle + \rho \mathbb{U} &= \langle \mathbf{y} \rangle + \rho \cdot \mathbf{A} \cdot \mathcal{E} \\ &\subset \langle \mathbf{y} \rangle + \rho \cdot \mathbf{A} \cdot [\mathcal{E}] \\ &= \mathbf{A} \cdot \begin{pmatrix} e_1 + \rho\sqrt{q_1} & 0 & \cdots & 0 \\ 0 & e_2 + \rho\sqrt{q_2} & & \vdots \\ \vdots & \ddots & & 0 \\ 0 & \cdots & 0 & e_m + \rho\sqrt{q_m} \end{pmatrix} \cdot \begin{pmatrix} [-1,1] \\ \vdots \\ [-1,1] \end{pmatrix}\end{aligned} \tag{27}$$

we get the enclosure to be proven. □

Example 1. *Consider the two dimensional case, where*

$$\mathbf{A} = \begin{pmatrix} \mathbf{a}_1 & \mathbf{a}_2 \end{pmatrix} = \begin{pmatrix} a_{11} & a_{21} \\ a_{12} & a_{22} \end{pmatrix} \tag{28}$$

We have

$$\mathbf{A}^T \cdot \mathbf{A} = \begin{pmatrix} \mathbf{a}_1^T \\ \mathbf{a}_2^T \end{pmatrix} \begin{pmatrix} \mathbf{a}_1 & \mathbf{a}_2 \end{pmatrix} = \begin{pmatrix} \|\mathbf{a}_1\|^2 & \mathbf{a}_1^T \mathbf{a}_2 \\ \mathbf{a}_1^T \mathbf{a}_2 & \|\mathbf{a}_2\|^2 \end{pmatrix} \tag{29}$$

We get

$$\mathbf{Q} = \left(\mathbf{A}^T \cdot \mathbf{A}\right)^{-1} = \frac{1}{\|\mathbf{a}_1 \wedge \mathbf{a}_2\|^2} \cdot \begin{pmatrix} \|\mathbf{a}_2\|^2 & \times \\ \times & \|\mathbf{a}_1\|^2 \end{pmatrix} \tag{30}$$

From Proposition 2, we get

$$\langle \mathbf{y} \rangle + \rho \mathbb{U} \subset \mathbf{A} \cdot \begin{pmatrix} e_1 + \rho \frac{\|\mathbf{a}_2\|}{\|\mathbf{a}_1 \wedge \mathbf{a}_2\|} & 0 \\ 0 & e_2 + \rho \frac{\|\mathbf{a}_1\|}{\|\mathbf{a}_1 \wedge \mathbf{a}_2\|} \end{pmatrix} \cdot \begin{pmatrix} [-1,1] \\ [-1,1] \end{pmatrix}. \tag{31}$$

2.3.3. Inflating a centered flat parallelepiped

Proposition 3. *Define the n dimensional flat parallelepiped*

$$\langle \mathbf{y} \rangle = \mathbf{A} \cdot \begin{pmatrix} [-e_1, e_1] \\ \vdots \\ [-e_m, e_m] \end{pmatrix} \tag{32}$$

where $m < n$. The matrix $\mathbf{A}$ is assumed to be full rank. Consider a matrix $\mathbf{N}$ such that the matrix $\tilde{\mathbf{A}} = [\mathbf{A}|\mathbf{N}]$ is square and invertible. Consider the

unit ball $\mathbb{U}$ *of* $\mathbb{R}^n$ *and an inflation coefficient* $\rho > 0$. *The parallelepiped of* $\mathbb{R}^n$*:*

$$\langle \mathbf{z} \rangle = \tilde{\mathbf{A}} \cdot \begin{pmatrix} e_1 + \rho\sqrt{q_1} & 0 & \cdots & 0 & 0 & 0 & 0 \\ 0 & e_2 + \rho\sqrt{q_2} & & \vdots & 0 & 0 & 0 \\ \vdots & \vdots & \ddots & 0 & \vdots & 0 & 0 \\ 0 & \cdots & 0 & e_m + \rho\sqrt{q_m} & 0 & \vdots & 0 \\ 0 & 0 & & 0 & \rho\sqrt{q_{m+1}} & 0 & \vdots \\ 0 & 0 & 0 & \vdots & 0 & \ddots & 0 \\ 0 & 0 & 0 & 0 & \cdots & 0 & \rho\sqrt{q_n} \end{pmatrix} \cdot [-1, 1]^n, \tag{33}$$

where q_i *is the* i*th diagonal element of the matrix* $\mathbf{Q} = \left(\tilde{\mathbf{A}}^T \tilde{\mathbf{A}}\right)^{-1}$*, satisfies*

$$\langle \mathbf{z} \rangle \supset \langle \mathbf{y} \rangle + \rho\mathbb{U}. \tag{34}$$

Proof. We have

$$\begin{aligned} \langle \mathbf{y} \rangle &= \mathbf{A} \cdot \begin{pmatrix} [-e_1, e_1] \\ \vdots \\ [-e_m, e_m] \end{pmatrix} + \mathbf{N} \cdot \begin{pmatrix} [0, 0] \\ \vdots \\ [0, 0] \end{pmatrix} \\ &= \underbrace{[\mathbf{A}|\mathbf{N}]}_{=\tilde{\mathbf{A}}} \cdot \begin{pmatrix} [-e_1, e_1] \\ \vdots \\ [-e_m, e_m] \\ [-e_{m+1}, e_{m+1}] \\ \vdots \\ [-e_n, e_n] \end{pmatrix} \end{aligned} \tag{35}$$

where $e_{m+1} = \cdots = e_n = 0$. By Proposition 2,$\langle \mathbf{z} \rangle$ in (33) encloses $\langle \mathbf{y} \rangle + \rho\mathbb{U}$ which completes the proof. □

This inflation process is summarized in Algorithm 1.

Example 2. *Assume that we want to inflate by* ρ *the parallelepiped*

$$\langle \mathbf{y} \rangle = \underbrace{\begin{pmatrix} a_{11} & a_{21} \\ a_{12} & a_{22} \\ a_{13} & a_{23} \end{pmatrix}}_{=\mathbf{A}} \cdot [-1, 1]^2 \tag{36}$$

Algorithm 1 Parallelepiped inflation

Inputs: $\langle \mathbf{y} \rangle, \rho$ so that $\langle \mathbf{y} \rangle = \mathbf{A} \cdot \begin{pmatrix} [-e_1, e_1] \\ \vdots \\ [-e_m, e_m] \end{pmatrix}$

Output: $\langle \mathbf{z} \rangle$

Notation: Inflate($\langle \mathbf{z} \rangle, \rho$)

Algorithm:

$\mathbf{N} \leftarrow \text{NullSpace}(\mathbf{A})$
$\tilde{\mathbf{A}} \leftarrow [\mathbf{A}|\mathbf{N}]$
$\mathbf{Q} \leftarrow \left(\tilde{\mathbf{A}}^{\mathrm{T}} \tilde{\mathbf{A}}\right)^{-1}$
$\mathbf{M} \leftarrow 0^{n \times n}$
for $i = 1$ **to** $i = n$
    $\mathbf{M}(i,i) \leftarrow \rho \cdot \sqrt{\mathbf{Q}(i,i)}$
end for
for $i = 1$ **to** $i = m$
    $\mathbf{M}(i,i) \leftarrow \mathbf{M}(i,i) + e_i$
end for
$\langle \mathbf{z} \rangle \leftarrow \tilde{\mathbf{A}} \cdot \mathbf{M} \cdot [-1, 1]^n$

We have

$$\tilde{\mathbf{A}} = \begin{pmatrix} \mathbf{a}_1 & \mathbf{a}_2 & \mathbf{n} \end{pmatrix} \tag{37}$$

where $\mathbf{n} = \mathbf{a}_1 \wedge \mathbf{a}_2$. *We have*

$$\tilde{\mathbf{A}}^{\,T} \cdot \tilde{\mathbf{A}} = \begin{pmatrix} \mathbf{a}_1^T \\ \mathbf{a}_2^T \\ \mathbf{n}^T \end{pmatrix} \begin{pmatrix} \mathbf{a}_1 & \mathbf{a}_2 & \mathbf{n} \end{pmatrix} = \begin{pmatrix} \|\mathbf{a}_1\|^2 & \mathbf{a}_1^T \mathbf{a}_2 & 0 \\ \mathbf{a}_1^T \mathbf{a}_2 & \|\mathbf{a}_2\|^2 & 0 \\ 0 & 0 & \|\mathbf{n}\|^2 \end{pmatrix} \tag{38}$$

Since $\det \tilde{\mathbf{A}} = \|\mathbf{n}\|^2$, *we get*

$$\begin{aligned}
\mathbf{Q} = \left(\tilde{\mathbf{A}}^T \cdot \tilde{\mathbf{A}}\right)^{-1} &= \frac{1}{\|\mathbf{n}\|^4} \begin{pmatrix} \|\mathbf{a}_2\|^2\|\mathbf{n}\|^2 & \times & \times \\ \times & \|\mathbf{a}_1\|^2\|\mathbf{n}\|^2 & \times \\ \times & \times & \|\mathbf{a}_1\|^2\|\mathbf{a}_2\|^2 - \left(\mathbf{a}_1^T\mathbf{a}_2\right)^2 \end{pmatrix} \\
&= \begin{pmatrix} \frac{\|\mathbf{a}_2\|^2}{\|\mathbf{n}\|^2} & \times & \times \\ \times & \frac{\|\mathbf{a}_1\|^2}{\|\mathbf{n}\|^2} & \times \\ \times & \times & \frac{\|\mathbf{a}_1\|^2\|\mathbf{a}_2\|^2 - \left(\mathbf{a}_1^T\mathbf{a}_2\right)^2}{\|\mathbf{n}\|^4} \end{pmatrix} \\
&= \begin{pmatrix} \frac{\|\mathbf{a}_2\|^2}{\|\mathbf{n}\|^2} & \times & \times \\ \times & \frac{\|\mathbf{a}_1\|^2}{\|\mathbf{n}\|^2} & \times \\ \times & \times & \frac{1}{\|\mathbf{n}\|^2} \end{pmatrix}
\end{aligned} \tag{39}$$

Therefore

$$\begin{aligned}
\langle \mathbf{z} \rangle &= \tilde{\mathbf{A}} \cdot \begin{pmatrix} 1 + \rho\frac{\|\mathbf{a}_2\|}{\|\mathbf{n}\|} & 0 & 0 \\ 0 & 1 + \rho\frac{\|\mathbf{a}_1\|}{\|\mathbf{n}\|} & 0 \\ 0 & 0 & \rho\frac{1}{\|\mathbf{n}\|} \end{pmatrix} \cdot [-1,1]^3 \\
&= \begin{pmatrix} (1 + \rho\frac{\|\mathbf{a}_2\|}{\|\mathbf{n}\|})\mathbf{a}_1 & (1 + \rho\frac{\|\mathbf{a}_1\|}{\|\mathbf{n}\|})\mathbf{a}_2 & \rho\frac{\mathbf{n}}{\|\mathbf{n}\|} \end{pmatrix} \cdot [-1,1]^3
\end{aligned} \tag{40}$$

An illustration is given by Figure 5.

2.3.4. Non centered case

Consider the flat parallelepiped

$$\langle \mathbf{y} \rangle = \langle \mathbf{y}_c \rangle + \bar{\mathbf{y}} \tag{41}$$

where $\langle \mathbf{y}_c \rangle$ is a parallelepiped with center $\mathbf{0}$. To inflate $\langle \mathbf{y} \rangle$ by ρ, we inflate $\langle \mathbf{y}_c \rangle$ as explained in Proposition 3 and then, we translate by $\bar{\mathbf{y}}$.

2.4. Parallelepiped inclusion function

Proposition 4. *Given* $\mathbf{f} : \mathbb{R}^m \mapsto \mathbb{R}^n$ *with* $m < n$. *A parallelepiped inclusion function is given by :*

$$\begin{array}{rccc} \langle \mathbf{f} \rangle : & \mathbb{IR}^m & \mapsto & \mathbb{PR}^n \\ & [\mathbf{x}] & \to & \langle \mathbf{f} \rangle([\mathbf{x}]) = \bar{\mathbf{y}} + \mathbf{A} \cdot [-1,1]^n \end{array} \tag{42}$$

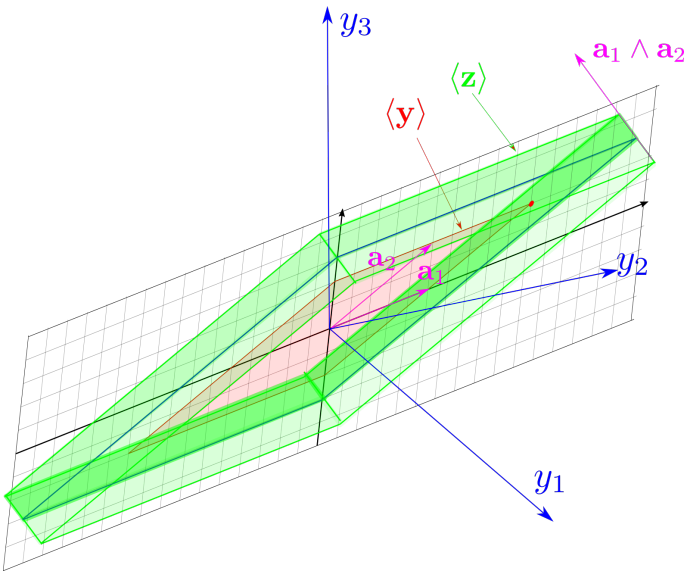

Figure 5: Inflation of the flat parallelepiped $\langle \mathbf{y} \rangle$

with

$$\begin{array}{rcl} \bar{\mathbf{y}} & = & \mathbf{f}(\bar{\mathbf{x}}) \\ \mathbf{A} & = & \mathit{Inflate}(\frac{d\mathbf{f}}{d\mathbf{x}}(\bar{\mathbf{x}}), \rho_{\mathbf{f}}([\mathbf{x}])) \\ \bar{\mathbf{x}} & = & \mathit{center}([\mathbf{x}]) \end{array} \tag{43}$$

where the Inflate function is described by Algorithm 1.

Proof. A first order Taylor approximation of $\mathbf{f}(\mathbf{x})$ is

$$\mathbf{f}(\mathbf{x}) \simeq \underbrace{\mathbf{f}(\bar{\mathbf{x}}) + \frac{d\mathbf{f}}{d\mathbf{x}}(\bar{\mathbf{x}}) \cdot (\mathbf{x} - \bar{\mathbf{x}})}_{\ell(\mathbf{x})}$$

Now, from Theorem 1 the error made by this approximation when $\mathbf{x} \in [\mathbf{x}]$ is lower than $\rho_{\mathbf{f}}([\mathbf{x}])$. The inflation has thus to be performed as defined in Algorithm 1 . This yields the expression for $\mathbf{A}$. The translation by $\bar{\mathbf{y}}$ is explained in Subsection 2.3.4. □

The following section shows that the parallelepiped inclusion function has a nice property of convergence.

3. Parallelepiped enclosure of the image of a large box

The previous section has shown how to compute a parallelepiped which accurately encloses the image of a tiny box $[\mathbf{x}]$ by a function $\mathbf{f} : \mathbb{R}^m \mapsto \mathbb{R}^n$. When the box $[\mathbf{x}]$ is large, it has to be cut into small subboxes. We will show that we can obtain an accurate outer approximation and quantify the quality of the approximation in terms of convergence order. The corresponding methodology will be used later in Section 5 to get both an inner and an outer approximations of the image set in the case where $m = n$.

3.1. Principle

Consider a function $\mathbf{f} : \mathbb{R}^m \mapsto \mathbb{R}^n$ with $m < n$ and a box $[\mathbf{x}]$ of $\mathbb{R}^m$. We want to compute an accurate parallelepiped approximation which encloses $\mathbf{f}([\mathbf{x}])$. Equivalently, we want to compute a collection of parallelepipeds the union of which contains $\mathbf{f}([\mathbf{x}])$.

To achieve our goal, we cut the box $[\mathbf{x}]$ into small boxes $\{[\mathbf{x}](0), [\mathbf{x}](1), \dots\}$. Then, for each of these boxes $[\mathbf{x}](i)$, we compute a parallelepiped $\langle\mathbf{f}\rangle([\mathbf{x}](i))$ containing the set $\mathbf{f}([\mathbf{x}](i))$.

3.2. Order

Definition 4. Given $\mathbf{f} : \mathbb{R}^m \mapsto \mathbb{R}^n$ a C^1 function with $m < n$. The inclusion function $\langle\mathbf{f}\rangle$ converges with an order k, if for any tiny box $[\mathbf{x}]$, we have

$$\mathrm{vol}(\langle\mathbf{f}\rangle([\mathbf{x}])) = \varepsilon^n \varepsilon^{k(n-m)} \tag{44}$$

where we use the asymptotic Bachmann–Landau notation [29]: $\varepsilon = O(w([\mathbf{x}]))$ (see below). The *order of convergence* of $\langle\mathbf{f}\rangle$ is the largest k such that $\langle\mathbf{f}\rangle$ converges with an order k.

To understand this definition, consider the following points.

1. The notation with ε is needed to shorten the mathematics expressions, but should be handled with care. When we write $\phi([\mathbf{x}]) = \varepsilon^i$. It means that $\phi([\mathbf{x}]) \in \mathbb{R}$ and that if we take a nested sequence $[\mathbf{x}](i)$ converging to $\bar{\mathbf{x}} \in \mathbb{R}$, the ratio $\frac{\phi([\mathbf{x}])}{w([\mathbf{x}])^i}$ remains bounded. For instance, if $\mathbf{f} : \mathbb{R}^m \mapsto \mathbb{R}^n$ and if $[\mathbf{f}]$ is the natural inclusion function for $\mathbf{f}$, we can write $w([\mathbf{x}]) = \varepsilon$, $\mathrm{vol}([\mathbf{x}]) = \varepsilon^m$,$w([\mathbf{f}]([\mathbf{x}])) = \varepsilon$ and $\mathrm{vol}([\mathbf{f}]([\mathbf{x}])) = \varepsilon^n$.

2. If $m = n$, Definition 4 does not apply. It is important to have $\text{vol}(\mathbf{f}([\mathbf{x}])) = 0$ (*i.e.*, $m < n$) to be able to define the order of convergence. The order of convergence becomes essential as soon as $n - m > 0$. In the applications of this paper, we will take $n - m = 1$.
3. If $[\mathbf{f}]$ is the natural inclusion function, we know [12], that

$$\text{vol}([\mathbf{f}]([\mathbf{x}])) = \varepsilon^n. \tag{45}$$

   Thus the natural inclusion function has an order 0.
4. A logarithmic view of (44) is

$$\log\left(\text{vol}(\langle\mathbf{f}\rangle([\mathbf{x}]))\right) = (n + k(n - m))\log\varepsilon \tag{46}$$

   Thus, if we draw for tiny boxes $\log\left(\text{vol}(\langle\mathbf{f}\rangle([\mathbf{x}]))\right)$ as a function of $\log\varepsilon$ we should observe an asymptotic behavior when $\varepsilon \to 0$.

Proposition 5. *If* $\mathbf{f}$ *is of class* C^1 *, the parallelepiped inclusion function is of order* $k = 1$.

This proposition is illustrated by Figure 6 in the situation where $m = 1$ and $n = 2$. We have $w([\mathbf{x}]) = \varepsilon$, and $\text{vol}([\mathbf{f}]([\mathbf{x}])) = \varepsilon^2$ and $\text{vol}(\langle\mathbf{f}\rangle([\mathbf{x}])) = \varepsilon^3$.

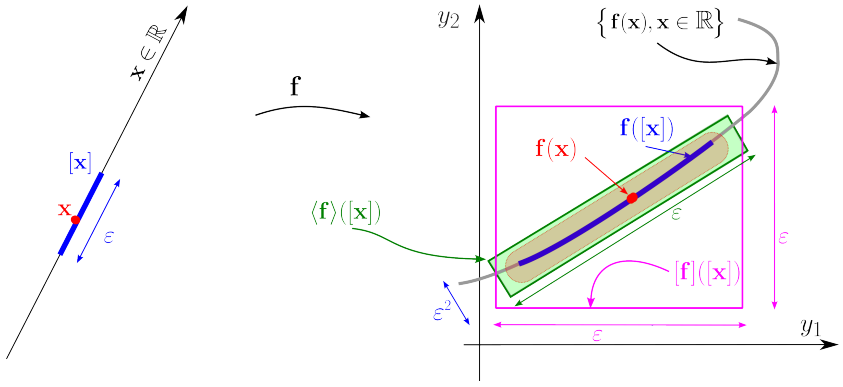

Figure 6: Illustration of the convergence order in ε^3 of $\langle\mathbf{f}\rangle$ for $m = 1$ and $n = 2$

Proof. Consider a tiny box $[\mathbf{x}]$ with center $\bar{\mathbf{x}}$. We have

$$\begin{array}{rcl} w\left(\left[\frac{d\mathbf{f}}{d\mathbf{x}}\right]([\mathbf{x}]) - \frac{d\mathbf{f}}{d\mathbf{x}}(\bar{\mathbf{x}})\right) & = & \varepsilon \\ w\left([\mathbf{x}] - \bar{\mathbf{x}}\right) & = & \varepsilon \end{array} \tag{47}$$

As a consequence (see [30])

$$\begin{array}{rcl} & w\left(\left(\left[\frac{d\mathbf{f}}{d\mathbf{x}}\right]([\mathbf{x}]) - \frac{d\mathbf{f}}{d\mathbf{x}}(\bar{\mathbf{x}})\right) \cdot ([\mathbf{x}] - \bar{\mathbf{x}})\right) & = & \varepsilon^2 \\ \Rightarrow & \left\|\left(\left[\frac{d\mathbf{f}}{d\mathbf{x}}\right]([\mathbf{x}]) - \frac{d\mathbf{f}}{d\mathbf{x}}(\bar{\mathbf{x}})\right) \cdot ([\mathbf{x}] - \bar{\mathbf{x}})\right\| & = & \varepsilon^2 \\ \Rightarrow & \rho([\mathbf{x}]) = \mathrm{ub}\left(\left\|\left(\left[\frac{d\mathbf{f}}{d\mathbf{x}}\right]([\mathbf{x}]) - \frac{d\mathbf{f}}{d\mathbf{x}}(\bar{\mathbf{x}})\right) \cdot ([\mathbf{x}] - \bar{\mathbf{x}})\right\|\right) & = & \varepsilon^2 \end{array} \tag{48}$$

This is a well known property of the centered form already shown in [12]. Now, due to our inflation process, we have

$$\mathrm{vol}(\langle \mathbf{f} \rangle([\mathbf{x}])) = \rho^{n-m}([\mathbf{x}]) \cdot \varepsilon^m, \tag{49}$$

as illustrated by Figure 6 for $m = 1$ and $n = 2$. Since $\rho([\mathbf{x}]) = \varepsilon^2$, we have

$$\mathrm{vol}(\langle \mathbf{f} \rangle([\mathbf{x}])) = \varepsilon^{2(n-m)} \cdot \varepsilon^m = \varepsilon^n \varepsilon^{1(n-m)} \tag{50}$$

which concludes the proof. □

3.3. Accuracy of the approximation

Consider a large box $[\mathbf{x}]$ and cut it into small boxes $\{[\mathbf{x}](i), i \in \{1, 2, \dots\}\}$ of width $\varepsilon = o(w([\mathbf{x}]))$. We have approximately ε^{-m} subboxes covering $[\mathbf{x}]$. Our parallelepiped approximation $\langle \mathbf{f} \rangle([\mathbf{x}](i)) \subset \mathbb{R}^n$ has a strictly positive volume V (to be understood as a n-dimensional Lebesgue measure), whereas the volume of the set $\mathbf{f}([\mathbf{x}])$ is zero since $m < n$. The volume V satisfies

$$\begin{array}{rcll} \log V & = & \log\left(\mathrm{vol}(\langle \mathbf{f} \rangle([\mathbf{x}](i))) \cdot \varepsilon^{-m}\right) & \\ & = & \log\left(\mathrm{vol}(\langle \mathbf{f} \rangle([\mathbf{x}](i)))\right) - m \log \varepsilon & \\ & = & (n + k(n-m)) \log \varepsilon - m \log \varepsilon & \text{See (46)} \\ & = & (k+1)(n-m) \log \varepsilon & \end{array} \tag{51}$$

Since $k = 1$ for the parallelepiped approximation, we get

$$\log V_{\langle \mathbf{f} \rangle} = 2(n-m) \log \varepsilon \tag{52}$$

Since $k = 0$ for any interval approximation, we get

$$\log V_{[\mathbf{f}]} = (n-m) \log \varepsilon \tag{53}$$

The parallelepiped approximation provides a better convergence order if

$$\begin{array}{rc} & \log V_{\langle \mathbf{f} \rangle} < \log V_{[\mathbf{f}]} \\ \Leftrightarrow & (2n - 2m) \log \varepsilon < (n-m) \log \varepsilon \\ \Leftrightarrow & 2n - 2m > n - m \\ \Leftrightarrow & n > m \end{array} \tag{54}$$

The parallelepiped approximation becomes interesting as soon as $n > m$. To solve the direct problem for $\mathbf{f} : \mathbb{R}^n \mapsto \mathbb{R}^n$, the boundary approach allows us to decrease the dimension of $\mathbf{x}$ by one (*i.e.*, $m = n - 1$). This justifies the combination of the boundary approach and the parallelepiped approximation.

Remark 4. We have chosen to quantify the convergence in terms of volume, but the Hausdorff distance could have been used as well for this comparison. A similar result would have been obtained.

3.4. Example

Assume that we want to enclose the set $\boldsymbol{\psi}_0([\mathbf{x}])$ with $[\mathbf{x}] = [-1, 1]^2$ and

$$\boldsymbol{\psi}_0(\mathbf{x}) = \begin{pmatrix} \frac{1}{\sqrt{1+x_1^2+x_2^2}} \\ \frac{x_1}{\sqrt{1+x_1^2+x_2^2}} \\ \frac{x_2}{\sqrt{1+x_1^2+x_2^2}} \end{pmatrix} \tag{55}$$

which corresponds to the *inverse gnomonic chart* that will be reconsidered later. The set $\boldsymbol{\psi}_0([\mathbf{x}])$ is painted red in Figure 7(a). Since $\|\boldsymbol{\psi}_0(\mathbf{x})\| = 1$, the red surface is a part of the unit sphere of $\mathbb{R}^3$. The Jacobian matrix is

$$\frac{d\boldsymbol{\psi}_0}{d\mathbf{x}} = \frac{1}{\sqrt{1 + x_1^2 + x_2^2}^3} \begin{pmatrix} -x_1 & -x_2 \\ 1 + x_2^2 & -x_1 x_2 \\ -x_1 x_2 & 1 + x_1^2 \end{pmatrix}. \tag{56}$$

We can thus get the parallelepiped approximation. For $\varepsilon = 0.2$, we obtain Figure 7(b) with a pessimism of $\rho = 0.22$. For $\varepsilon = 0.1$, we obtain Figure 7(c) with $\rho = 0.051$. For $\varepsilon = 0.05$, we get Figure 7(d) with $\rho = 0.012$.

4. Gnomonic atlas

In the previous section, we have shown how to compute an outer approximation of the image of a large box by a nonlinear function $\mathbf{f} : \mathbb{R}^m \to \mathbb{R}^n$, $m < n$. Now, in this paper, we want to compute an *inner* and an *outer* approximation of the image $\mathbb{Y} = \mathbf{f}(\mathbb{X})$ of a set $\mathbb{X}$ in the case where $m = n$. The set $\mathbb{X}$ can have any shape (*e.g.*, a ball), but it is assumed to be compact and to have a boundary $\mathbb{M} = \partial\mathbb{X}$ which is a smooth manifold of dimension $n - 1$. This assumption is needed to use our boundary approach. An atlas [31] covering $\mathbb{M}$ can be built. Now, to be able to use the results of the

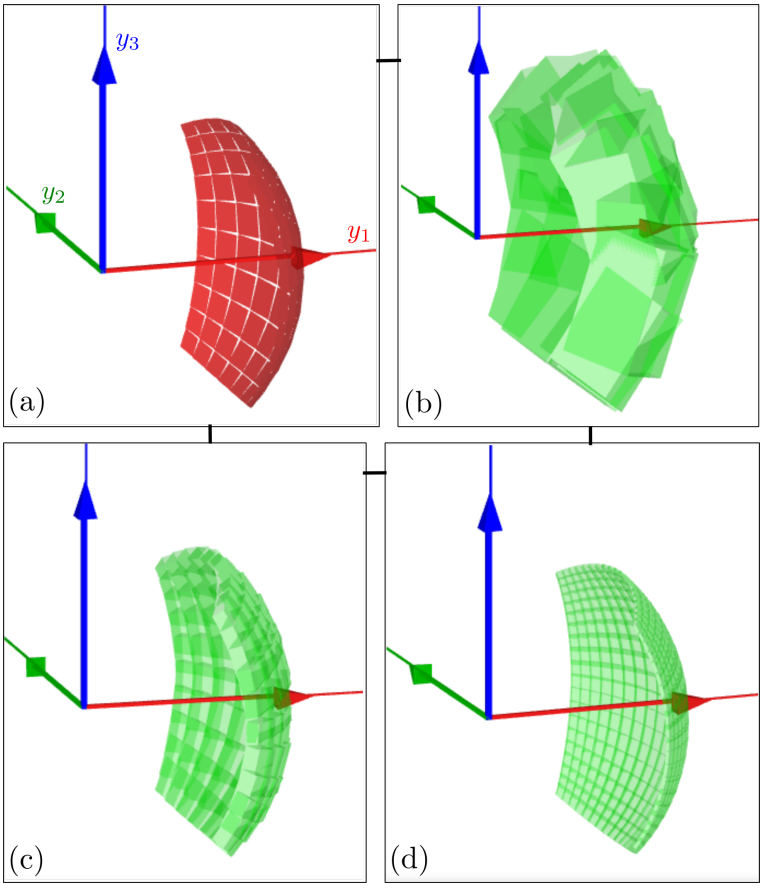

Figure 7: Approximation of $\boldsymbol{\psi}_0([-1,1]^2)$

previous section, the atlas for $\mathbb{M}$ should be a *box-atlas* [32, 23], *i.e.*, an atlas whose charts domains are boxes. The construction of the charts can be facilitated using symmetries. As shown in [23], box atlas can be built for several manifolds: spheres, Lie groups such as SO(3), ... To our knowledge, characterizing the class of manifolds for which a box atlas exists is still an open problem.

This section defines the notion of gnomonic atlas which is a box-atlas that can be defined by a unique chart. All other charts can be deduced using symmetries. An illustration will be defined in the case where $\mathbb{M}$ is a sphere of $\mathbb{R}^3$. Note that the corresponding atlas needs to be constructed specifically for the sphere as a special case.

4.1. Gnomonic projection

The gnomonic projection, represented by Figure 8, is one possible projection used to map the Earth. All great circles map to straight lines of the chart and large distortion occur far from the center. This projection will be used to cut the unit sphere into similar regions called *quarters*.

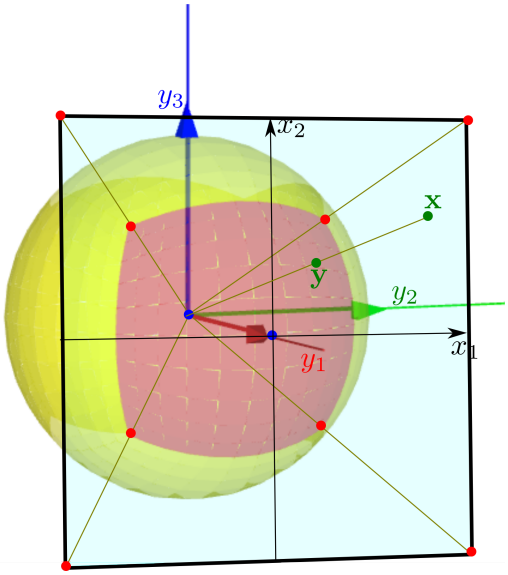

Figure 8: Gnomonic projection of the red gnomonic quarter onto the box $[-1,1]^2$

4.2. Box atlas

To cover the whole sphere, we can consider six gnomonic charts. As illustrated by Figure 9, we have an atlas of the sphere, which is called a *box atlas*. A *box atlas* [32] on a manifold $\mathbb{M}$ of dimension m is a family of pairs $\{(\mathbb{U}_i, \boldsymbol{\varphi}_i), i \in \{1, \ldots, i_{\max}\}\}$ such that $\mathbb{U}_1 \cup \cdots \cup \mathbb{U}_{i_{\max}} = \mathbb{M}$. The $\mathbb{U}_i$ are compact sets and are such that their interior do not overlap. The $\boldsymbol{\varphi}_i$ (called the charts) are invertible and $\boldsymbol{\varphi}_i(\mathbb{U}_i) = [-1,1]^m$.

4.3. Using symmetries

In the example of the sphere, all charts can be obtained from one of them using symmetries (or action) and one chart. This is illustrated by Figure 10 where $\boldsymbol{\psi}_0 = \boldsymbol{\varphi}_0^{-1}$. Indeed, from one of the six quarters of the sphere we can generate all other quarters. Two generators are needed. We can take

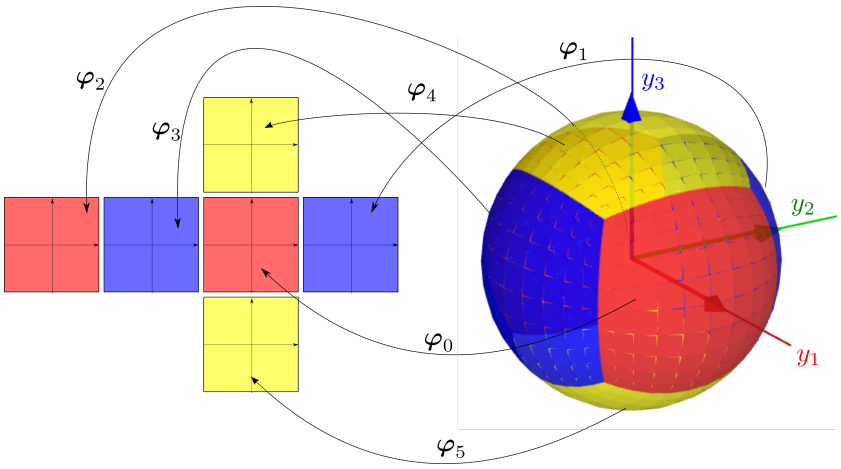

Figure 9: 6 charts of the sphere

for instance $s_1 = e^{\mathbf{k}\cdot\frac{\pi}{2}}$ the rotation of $\frac{\pi}{2}$ with respect to $\mathbf{k}$ (the y_3 axis) and $s_2 = e^{\mathbf{j}\cdot\frac{\pi}{2}}$ the rotation of $\frac{\pi}{2}$ with respect to $\mathbf{j}$ (the y_2 axis). The six symmetry actions that are needed to cover the sphere are

$$\Sigma = \left\{1, s_1, s_1^2, s_1^{-1}, s_2, s_2^{-1}\right\}. \tag{57}$$

We can thus write that the sphere corresponds to the set

$$\mathbb{S} = \bigcup_{\sigma\in\Sigma} \sigma \circ \boldsymbol{\psi}_0([-1,1]^2). \tag{58}$$

Definition 5. Given a manifold $\mathbb{M} \subset \mathbb{R}^n$ of dimension m. A *gnomonic atlas* $\{\boldsymbol{\psi}_0, \Sigma\}$ for a manifold $\mathbb{M}$ is composed of the inverse chart $\boldsymbol{\psi}_0$ and a set of symmetries Σ of $\mathbb{R}^n$ such that

$$\mathbb{M} = \bigcup_{\sigma\in\Sigma} \sigma \circ \boldsymbol{\psi}_0([-1,1]^m). \tag{59}$$

Moreover, the quarter $\sigma \circ \boldsymbol{\psi}_0([-1,1]^m)$, $\sigma \in \Sigma$ should not have overlapping interiors.

5. Computing the image of a set by a nonlinear $\mathbb{R}^n \to \mathbb{R}^n$ function

Consider a C^1 function $\mathbf{f} : \mathbb{R}^n \to \mathbb{R}^n$ and a compact set $\mathbb{X}$. Its boundary $\mathbb{M} = \partial\mathbb{X}$ is assumed to be a smooth, compact manifold $\mathbb{M}$ of $\mathbb{R}^n$.

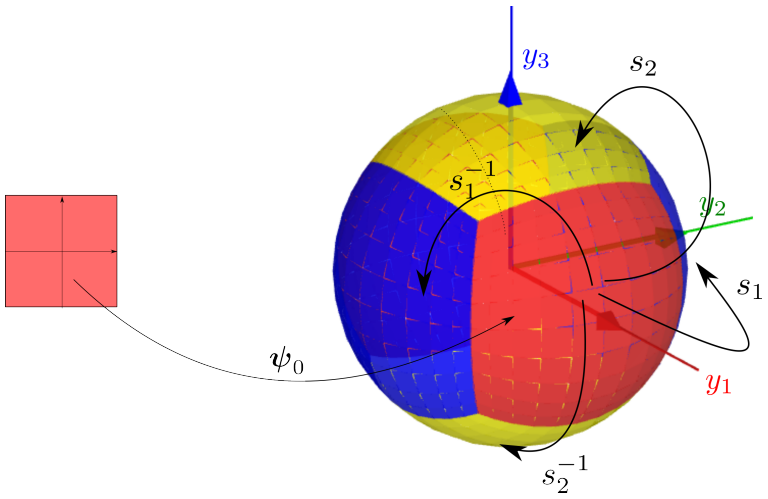

Figure 10: The sphere can be generated by a unique chart and 6 symmetries

We say $\mathbf{f}$ is locally injective at a point $\mathbf{x}_0 \in \mathbb{X}$ if it is injective on some neighbourhood of $\mathbf{x}_0$; it is locally injective on $\mathbb{X}$ if it is locally injective at each point of $\mathbb{X}$. By the Inverse Function Theorem, if $\mathbf{f}$ is $\mathcal{C}^1$ and the Jacobian $\mathbf{f}'(x)$ is nonsingular at $\mathbf{x}_0$ then f has a $\mathcal{C}^1$ inverse in a neighbourhood of $\mathbf{x}_0$ and in particular is locally injective.

In this case, an inner and an outer approximations of $\mathbb{Y} = \mathbf{f}(\mathbb{X})$ can be obtained by computing an enclosure for $\mathbf{f}(\mathbb{M})$.

Example 3. *Take* $f(x) = x^2$ *and* $\mathbb{X}_1 = [2, 3]$. *We have* $\mathbb{M}_1 = \{2, 3\}$, $f(\mathbb{M}_1) = \{4, 9\}$ *and* $f(\mathbb{X}_1) = [4, 9]$, *which illustrates the fact that* $f(\mathbb{X}_1)$ *can be deduced from* $f(\mathbb{M}_1)$. *The condition of local injectivity is valid, since* $\frac{df}{dx}(x) \neq 0, \forall x \in \mathbb{X}_1$. *If we now take* $\mathbb{M}_2 = \{-2, 3\}$. *We have* $f(\mathbb{M}_2) = \{4, 9\}$ *whereas* $f(\mathbb{X}_2) = [0, 9]$. *There is a fold at* $x = 0$ *and* $f(\mathbb{X}_2)$ *cannot be deduced from* $f(\mathbb{M}_2)$. *The condition of local injectivity is not valid, since* $\frac{df}{dx}(0) = 0$.

In this section, we explain how this boundary approach can be implemented and illustrate why it is interesting in terms of convergence order.

If $\mathbf{f}$ is locally injective, from [33], we have: $\partial\mathbb{Y} \subset \mathbf{f}(\mathbb{M})$. If it is not case, we may have folds that contribute to $\partial\mathbb{Y}$. Since we assume the local injectivity of $\mathbf{f}$, to get an inner and an outer approximations of $\mathbb{Y}$, it is enough to compute an outer enclosure for $\mathbf{f}(\mathbb{M})$. We thus get an outer enclosure for $\partial\mathbb{Y}$ from which we can deduce an inner and an outer approximations for $\mathbb{Y}$. Indeed, the $\partial\mathbb{Y}$ separates the space into two zones: $\mathbb{Y}$ and its complementary $\overline{\mathbb{Y}}$. Only

the set $\mathbb{Y}$ is bounded, which allows us to know which zone is $\mathbb{Y}$ and which one is $\overline{\mathbb{Y}}$. The classification can be done using the Alexander rules [34].

For a given set $\mathbb{X} \subset \mathbb{R}^n$, the topological boundary $\mathbb{M}$ of $\mathbb{X}$, is defined as

$$\mathbb{M} = \partial\mathbb{X} = \overline{\mathbb{X}} \backslash \text{int}(\mathbb{X}) \tag{60}$$

where $\overline{\mathbb{X}}$ is the closure of $\mathbb{X}$ (*i.e.*, all points in $\mathbb{X}$ plus its limit points) and int($\mathbb{X}$), the interior of $\mathbb{X}$ (all points that have a neighborhood completely contained in $\mathbb{X}$).

Remark 5. We restrict our study to the case $\mathbf{f} : \mathbb{R}^m \to \mathbb{R}^n$ where $m = n$. The case where $m < n$ is less interesting since $\mathbb{Y} = \mathbf{f}(\mathbb{X})$ is an embedded manifold of $\mathbb{R}^n$ with a zero volume and no interior (and we are interested by the inner approximation). Our boundary approach can neither be interesting for the case where $m > n$ since we would have $\mathbb{Y} = \mathbf{f}(\mathbb{M})$ which gives no information on the boundary $\partial\mathbb{Y}$ of $\mathbb{Y}$ and thus no possibility to get an inner approximation of $\mathbb{Y}$.

5.1. Enclosing the image of a manifold

The following theorem explains how to compute an enclosure of the image $\mathbf{f}(\mathbb{M})$ by $\mathbf{f}$ of a manifold $\mathbb{M}$. For our application, $\mathbb{M} = \partial\mathbb{X}$.

Theorem 2. *Consider gnomonic atlas* $\{\boldsymbol{\psi}_0, \Sigma\}$ *of a manifold* $\mathbb{M} \subset \mathbb{R}^n$ *of dimension* m *and a function* $\mathbf{f} : \mathbb{R}^n \to \mathbb{R}^n$. *We have*

$$\mathbf{f}(\mathbb{M}) \subset \bigcup_i \langle \mathbf{g}_i \rangle([-1,1]^m) \tag{61}$$

where $\langle \mathbf{g}_i \rangle$ *is a parallelepiped inclusion function of*

$$\mathbf{g}_i = \mathbf{f} \circ \sigma_i \circ \boldsymbol{\psi}_0 \tag{62}$$

and σ_i is the ith element of Σ.

The construction of $\mathbf{g}_i([-1,1]^m)$ is illustrated by Figure 11.

Proof. Since $\{\boldsymbol{\psi}_0, \Sigma\}$ is a box atlas, we have

$$\mathbb{M} = \bigcup_i \sigma_i \circ \boldsymbol{\psi}_0([-1,1]^m) \tag{63}$$

Thus

$$\begin{array}{rcl} \mathbf{f}(\mathbb{M}) & = & \mathbf{f}\left(\bigcup_i \sigma_i \circ \boldsymbol{\psi}_0([-1,1]^m)\right) \\ & = & \bigcup_i \mathbf{f} \circ \sigma_i \circ \boldsymbol{\psi}_0([-1,1]^m) \\ & = & \bigcup_i \mathbf{g}_i([-1,1]^m) \end{array} \tag{64}$$

Now, $\mathbf{g}_i([-1,1]^m) \subset \langle \mathbf{g}_i \rangle([-1,1]^m)$ which concludes the proof. □

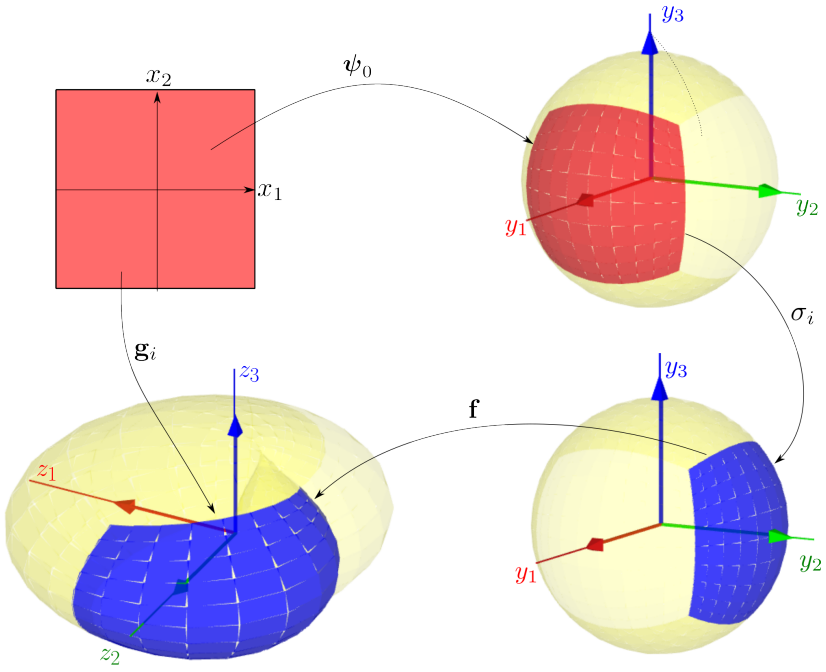

Figure 11: Construction of the function $\mathbf{g}_i$

5.2. Test-case 1

Consider the mapping

$$\mathbf{f}\begin{pmatrix} y_1 \\ y_2 \\ y_3 \end{pmatrix} \rightarrow \begin{pmatrix} y_1^2 - y_2^2 + y_1 \\ 2y_1y_2 + y_2 \\ y_3 \end{pmatrix} \tag{65}$$

This function has been built using complex polynomials to avoid folding. The two first components of this function correspond to the conformal mapping in $\mathbb{C}$ given by $z \mapsto z^2 + z$. Indeed

$$(y_1 + iy_2)^2 + (y_1 + iy_2) = y_1^2 - y_2^2 + y_1 + i(2y_1y_2 + y_2). \tag{66}$$

We want to compute the image $\mathbb{Z}$ of the unit ball

$$\mathbb{Y} = \left\{\mathbf{y} \in \mathbb{R}^3 \text{ such that } \|\mathbf{y}\| \leq 1\right\}. \tag{67}$$

We have

$$\frac{d\mathbf{f}}{d\mathbf{y}}(\mathbf{y}) = \begin{pmatrix} 2y_1 + 1 & -2y_2 & 0 \\ 2y_2 & 2y_1 + 1 & 0 \\ 0 & 0 & 1 \end{pmatrix}. \tag{68}$$

Since $\det \frac{d\mathbf{f}}{d\mathbf{y}}(\mathbf{y}) = (2y_1+1)^2 + 4y_2^2$, is nonzero except when $y_1 = -\frac{1}{2}$ and $y_2 = 0$, $\mathbf{f}$ has no fold on $\mathbb{Y}$. This means that the inside and the outside of $\mathbb{Z} = \mathbf{f}(\mathbb{Y})$ are separated by $\mathbf{f}(\partial\mathbb{Y})$ which makes our approach valid. Moreover, $\mathbf{f}$ tends to wrap $\mathbb{Y}$ into itself creating a continuum of self intersections. A parallelepiped approximation of $\mathbf{f}(\partial\mathbb{Y})$ has been computed by our algorithm. For $\varepsilon = 0.2$, the approach described in Section 5.1 generates Figure 12(b) with a pessimism of $\rho = 0.83$. For $\varepsilon = 0.1$, we obtain Figure 12(c) with $\rho = 0.18$. For $\varepsilon = 0.05$, we get Figure 12(d) with $\rho = 0.042$.

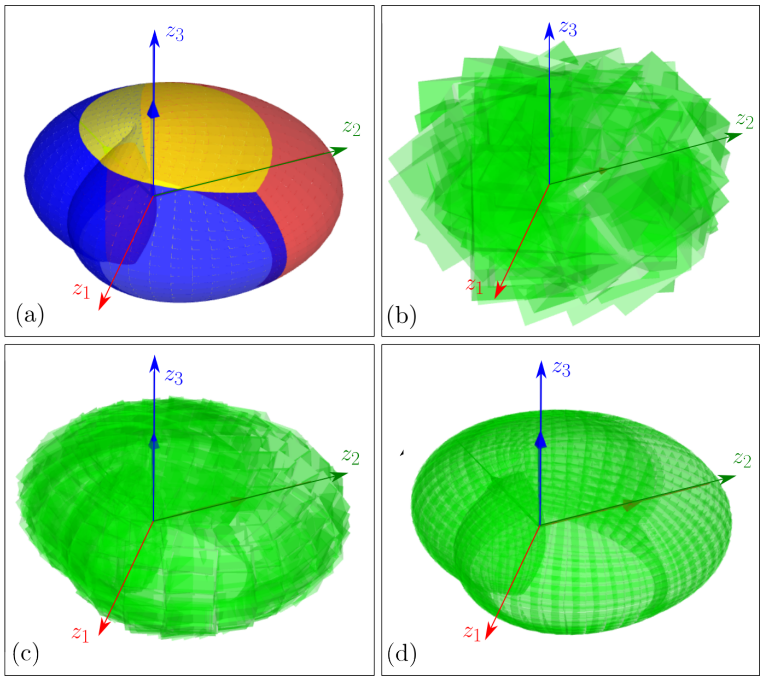

Figure 12: Covering of $\mathbf{f}(\mathbb{M})$ with parallelepipeds

5.3. Test-case 2

Consider the dynamical system

$$\dot{\mathbf{x}} = \boldsymbol{\gamma}(\mathbf{x}). \tag{69}$$

We define the flow $\boldsymbol{\Phi}_t(\mathbf{x}_0)$ as the function which returns the State vector $\mathbf{x}(t)$ reached at time t assuming that $\mathbf{x}(0)$ has been initialized at $\mathbf{x}_0$. More

formally, $\mathbf{\Phi}_t$ can be defined as the function:

$$\mathbf{\Phi}_t : \left\{ \begin{array}{ccc} \mathbb{R} \times \mathbb{R}^n & \rightarrow & \mathbb{R}^n \\ (t, \mathbf{x}) & \rightarrow & \mathbf{\Phi}_t(\mathbf{x}) \end{array} \right. \tag{70}$$

where

$$\begin{array}{c} \frac{d}{dt}\mathbf{\Phi}_t(\mathbf{x}) = \boldsymbol{\gamma}(\mathbf{\Phi}_t(\mathbf{x})) \\ \mathbf{\Phi}_0(\mathbf{x}) = \mathbf{x} \end{array} \tag{71}$$

Assume that $\mathbf{x}_0 \in \mathbb{X}_0$. For a given t, we define the *reach set* as

$$\mathbb{X}_t = \mathbf{\Phi}_t(\mathbb{X}_0). \tag{72}$$

We would like to use the parallelepiped method previously presented in order to characterize $\mathbb{X}_t$. Here $\mathbf{\Phi}_t$ plays the role of $\mathbf{f}$. Define $\mathbf{A}(\mathbf{x}_0, t) = \frac{\partial \mathbf{\Phi}_t(\mathbf{x}_0)}{\partial \mathbf{x}_0}$. If we integrate the *variational equation*

$$\dot{\mathbf{A}} = \frac{\partial \boldsymbol{\gamma}(\mathbf{x})}{\partial \mathbf{x}} \cdot \mathbf{A} \tag{73}$$

with $\mathbf{A}(0) = \mathbf{I}$ up to t, we get the Jacobian of $\mathbf{f}$. This Jacobian is needed to get a parallelepiped enclosure of $\mathbf{f}([\mathbf{x}])$. For interval evaluation of $\mathbf{f}$ and its Jacobian, we used the CAPD [35] combined with Codac [36].

As an illustration, we consider the Lorenz system

$$\begin{array}{rcl} \dot{x}_1 & = & 10(x_2 - x_1) \\ \dot{x}_2 & = & x_1(28 - x_2) - x_2 \\ \dot{x}_3 & = & x_1 x_2 - \frac{8}{3} x_3 \end{array} \tag{74}$$

An integration of the unit ball $\mathbb{X}_0$ for $t \in \{0, 0.05, 0.1, 0.15\}$, generates Figure 13. Quickly, we observe a strong distortion of the ball which is consistent with the chaotic behavior of the Lorenz system.

Let us now illustrate Formula (46) on our Lorenz example in order to visualize the convergence order of the approximation. For this, we take $t = 0.002$ and different precisions for the paving. Since $m = 2$ and $n = 3$, we get for the parallelepiped approximation (see (52)):

$$\log V_{\langle \mathbf{f} \rangle} = 2(n - m) \log \varepsilon = 2 \log \varepsilon \tag{75}$$

and for any interval extension (see (53)).

$$\log V_{[\mathbf{f}]} = (n - m) \log \varepsilon = \log \varepsilon. \tag{76}$$

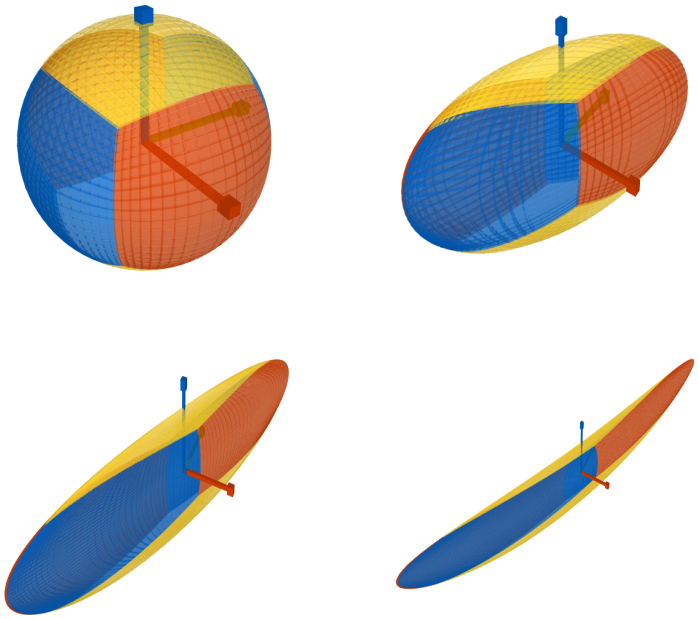

Figure 13: Covering of the reach set $\mathbb{X}_t$ with parallelepipeds for $t \in \{0, 0.05, 0.1, 0.15\}$

This is consistent with our numerical experiments depicted in Figure 14. The x axis corresponds to $\log \varepsilon$ and the y axis corresponds to the volume of the approximations. The blue box illustrates an asymptotic slope $\frac{\log V_{[\mathbf{f}]}}{\log \varepsilon}$ of 1 and the orange boxes illustrates an asymptotic slope $\frac{\log V_{\langle \mathbf{f} \rangle}}{\log \varepsilon}$ of 2.

5.4. Test-case 3

We chose here an example with a two dimensional solution set $\mathbb{Z}$. This makes the visualization of the inner and the outer approximations easier. Consider the mapping

$$\mathbf{f}\begin{pmatrix} y_1 \\ y_2 \end{pmatrix} \to \begin{pmatrix} y_1^2 - y_2^2 + y_1 \\ 2y_1y_2 + y_2 \end{pmatrix} \tag{77}$$

which is a two dimensional version of Test-case 1 (see (65)). We want to illustrate the occurrence of fake boundaries in $\mathbb{Z} = \mathbf{f}(\mathbb{Y})$ and how they could be avoided. Fake boundaries are symptomatic of boundary-based methods. When the studied function $\mathbf{f} : \mathbb{R}^n \to \mathbb{R}^n$ has no fold (like the function of Equation 77) we have

$$\partial\mathbb{Z} \subseteq \mathbf{f}(\partial\mathbb{Y}) \tag{78}$$

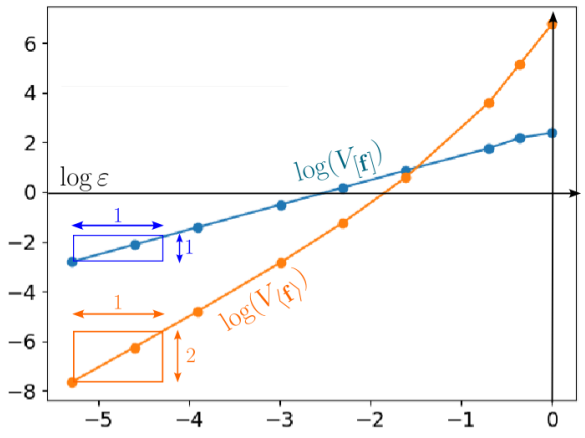

Figure 14: Order of approximation in terms of volumes with respect to $\log \varepsilon$ using parallelepipeds (orange) and a classical interval approach (blue)

The fake boundary is the set difference between $\mathbf{f}(\partial\mathbb{Y})$ and $\partial\mathbb{Z}$.

$$\mathbf{f}(\partial\mathbb{Y})\backslash\partial\mathbb{Z} = \{\mathbf{z} \in \mathbf{f}(\partial\mathbb{Y}) \,|\, \mathbf{z} \notin \partial\mathbb{Z}\}\,. \tag{79}$$

It occurs when $\mathbf{f}(\mathbb{Y})$ overlaps itself, *i.e.*, when $\mathbf{f}$ is not globally injective.

Let us compute the image $\mathbb{Z}$ of the unit disk

$$\mathbb{Y} = \left\{\mathbf{y} \in \mathbb{R}^2 \text{ such that } \|\mathbf{y}\| \leq 1\right\}. \tag{80}$$

Since $m = 1$, we can take the gnomonic atlas $\{\boldsymbol{\psi}_0, \Sigma\}$ with

$$\psi_0(x) = \begin{pmatrix} \cos\frac{\pi x}{4} \\ \sin\frac{\pi x}{4} \end{pmatrix} \tag{81}$$

and

$$\Sigma = \{1, s, s^2, s^3\} \tag{82}$$

where s is a rotation of $\pi/2$. For $\varepsilon = 0.2$, the approach described in Section 5.1 generates 40 parallelepipeds. We used the CGAL library to get the triangulation represented on the left of Figure 15. We observe that our approach which is based on the characterization of $\mathbf{f}(\partial\mathbb{Y})$ yields a fake boundary. This fake boundary corresponds to $\mathbf{f}(\partial\mathbb{Y})\backslash\partial\mathbf{f}(\mathbb{Y})$. Indeed, due to the local injectivity, the boundary $\partial\mathbb{Z}$ of the solution set $\mathbb{Z} = \mathbf{f}(\mathbb{Y})$ corresponds to $\partial\mathbf{f}(\mathbb{Y})$ which is a subset of $\mathbf{f}(\partial\mathbb{Y})$.

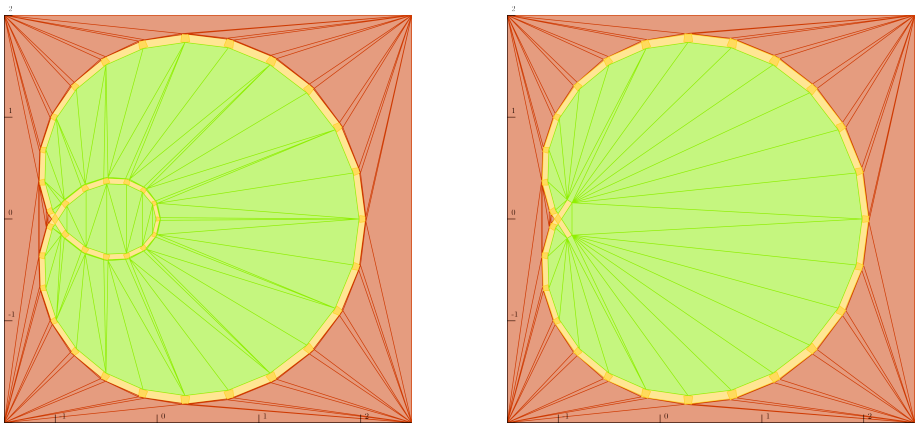

Figure 15: Triangulation approximation of $\mathbb{Z} = \mathbf{f}(\mathbb{Y})$ with (left) and without (right) the fake boundaries. The parallelepiped enclosing $\mathbf{f}(\partial\mathbb{Y})$ are painted yellow. The green triangles are inside $\mathbb{Z}$. The red triangles are outside $\mathbb{Z}$.

Now, parallelepipeds surrounded by green triangles are necessary inside $\mathbb{Z}$ and correspond to fake boundaries. This means that these parallelepipeds enclose elements of $\mathbf{f}(\partial\mathbb{Y})$ that are outside $\partial\mathbf{f}(\mathbb{Y})$. They could thus be removed to get the approximation for $\mathbf{f}(\mathbb{Y})$ on the right of Figure 15.

Let us note that in this example the function $\mathbf{f}$ is locally injective for all $\mathbf{y}$, except for $\mathbf{y}_0 = (-\frac{1}{2}, 0)$. To be totally rigorous, Equation 78 should then have been $\partial\mathbb{Z} \subseteq \mathbf{f}(\partial\mathbb{Y}) \cup \mathbf{f}(\mathbf{y}_0)$. Now it has to be noted that $\mathbf{f}(\mathbf{y}_0)$ is a single point. Due to the continuity of $\mathbf{f}$, we already know that $\partial\mathbb{Z}$ will not contain an isolated point. This assumption allows us to consider Equation 78 here.

6. Conclusion

In this paper, we have proposed an original approach to compute an inner and and outer approximations for a set $\mathbb{Y}$ defined as the image of a set $\mathbb{X}$ by nonlinear function $\mathbf{f} : \mathbb{R}^n \to \mathbb{R}^n$. This problem is fundamental as soon as we want to propagate uncertainties in a set-membership framework.

Our approach assumes that $\mathbf{f}$ is locally injective and that the boundary of $\mathbb{X}$ can be covered by a gnomonic atlas. The principle is to cover $\partial\mathbf{f}(\mathbb{X})$, the boundary of $\mathbf{f}(\mathbb{X})$, by small parallelepipeds. Each parallelepiped is computed using a linearisation followed by an inflation. The inflation rate is evaluated using the centered form provided by interval arithmetic to guarantee the enclosure.

An extension to the situation where $\mathbf{f} : \mathbb{R}^m \to \mathbb{R}^n$ is a submersion (*i.e.*, $m > n$) could be obtained using our parallelepiped approach by adding a projection step. As shown in [37], the case $m > n$ has several fundamental applications as in reachability analysis (see, *e.g.*, [38]).

The code source associated with the three test-cases is available at

https://godardma.github.io/subpages/libs/parallelepiped.html

References

[1] A. Papoulis, Probability, Random Variables, and Stochastic Processes, McGraw-Hill, New York, 1984.

[2] A. Dempster, The dempster-shafer calculus for statisticians, International Journal of Approximate Reasoning 48 (2008) 365–377.

[3] G. Nassreddine, F. Abdallah, T. Denoeux, State estimation using interval analysis and belief function theory: Application to dynamic vehicle localization, IEEE Transactions on Systems, Man, and Cybernetics 5 (40) (2010) 1205–1218.

[4] D. Dubois, H. Prade, Possibility Theory, Plenum, New York, 1988.

[5] E. Fogel, Y. F. Huang, On the value of information in system identification - bounded noise case, Automatica 18 (2) (1982) 229–238.

[6] L. Jaulin, M. Kieffer, O. Didrit, E. Walter, Applied Interval Analysis, with Examples in Parameter and State Estimation, Robust Control and Robotics, Springer-Verlag, London, 2001. doi:10.1007/978-1-4471-0249-6_2.

[7] R. E. Kalman, A new approach to linear filtering and prediction problems, Transactions of the AMSE, Part D, Journal of Basic Engineering 82 (1960) 35–45.

[8] S. Thrun, W. Bugard, D. Fox, Probabilistic Robotics, MIT Press, Cambridge, M.A., 2005.

[9] J. Idier (Ed.), Bayesian Approach to Inverse Problems, ISTE Ltd and John Wiley & Sons Inc.

[10] V. Kreinovich, G. Dimuro, A. C. da Rocha Costa, Probabilities, intervals, what next ? extension of interval computations to situations with partial information about probabilities, in: 10th IMEKO TC7 International symposium, 2004.

[11] A. N. Kolmogorov, Foundations of the Theory of Probability, Chelsea Publishing Company, New York, 1950, translated from the original German edition (Grundbegriffe der Wahrscheinlichkeitsrechnung, 1933).

[12] R. Moore, Methods and Applications of Interval Analysis, Society for Industrial and Applied Mathematics, 1979. doi:10.1137/1.9781611970906.

[13] B. Kearfott, V. Kreinovich, Applications of interval computations: An introduction, in: Applied Optimization, Springer US, 1996, pp. 1–22. doi:10.1007/978-1-4613-3440-8_1.

[14] C. Combastel, A state bounding observer for uncertain non-linear continuous-time systems based on zonotopes, in: 44th IEEE Conference on Decision and Control, 2005.

[15] C. Durieu, B. Polyak, E. Walter, Ellipsoidal state outer-bounding for MIMO systems via analytical techniques, in: Proceedings of the IMACS—IEEE–SMC CESA'96 Symposium on Modelling and Simulation, Vol. 2, Lille, France, 1996, pp. 843–848.

[16] A. Rauh, L. Jaulin, A computationally inexpensive algorithm for determining outer and inner enclosures of nonlinear mappings of ellipsoidal domains, International Journal of Applied Mathematics and Computer Science 31 (3) (2021) 399–415. doi:10.34768/AMCS-2021-0027.

[17] V. Kreinovich, A. Lakeyev, J. Rohn, P. Kahl, Computational Complexity and Feasibility of Data Processing and Interval Computations, Vol. 10, Springer Science & Business Media, 2013.

[18] J. Rohn, NP-hardness results for linear algebraic problems with interval data, in: J. Herzberger (Ed.), Topics in Validated Computations, Elsevier, Amsterdam, the Netherlands, 1994, pp. 463–471.

[19] M. Kieffer, L. Jaulin, E. Walter, Guaranteed recursive nonlinear state bounding using interval analysis, International Journal of Adaptative Control and Signal Processing 16 (2002) 193–218.

[20] M. C. Vianna, E. Goubault, L. Jaulin, S. Putot, Estimating the coverage measure and the area explored by a line-sweep sensor on the plane, International Journal of Approximate Reasoning 169 (June 2024).

[21] J. Boissonnat, A. Ghosh, Manifold reconstruction using tangential delaunay complexes, Discrete & Computational Geometry 51 (1) (2014) 221–267. doi:10.1007/s00454-013-9557-2.
URL https://link.springer.com/article/10.1007/s00454-013-9557-2

[22] E. Aamari, C. Levrard, Stability and minimax optimality of tangential delaunay complexes for manifold reconstruction, Discrete & Computational Geometry 59 (4) (2018) 923–971. doi:10.1007/s00454-017-9962-z.
URL https://link.springer.com/article/10.1007/s00454-017-9962-z

[23] A. Ignazi, R. Guyonneau, S. Lagrange, S. Lahaye, Box atlas: An interval version of atlas, International Journal of Approximate Reasoning 183 (2025). doi:10.1016/j.ijar.2025.109441.

[24] J. Wan, S. Sharma, R. Sutton, Guaranteed state estimation for nonlinear discrete-time systems via indirectly implemented polytopic set computation, IEEE Transactions on Automatic Control 63 (12) (2018) 4317–4322.

[25] B. Martin, A. Goldsztejn, L. Granvilliers, C. Jermann, Certified parallelotope continuation for one-manifolds, SIAM Journal on Numerical Analysis 51 (6) (2013) 3373–3401. doi:10.1137/120902799.

[26] R. Lohner, Enclosing the solutions of ordinary initial and boundary value problems, in: E. Kaucher, U. Kulisch, C. Ullrich (Eds.), Computer Arithmetic: Scientific Computation and Programming Languages, BG Teubner, Stuttgart, Germany, 1987, pp. 255–286.

[27] L. Jaulin, Reliable minimax parameter estimation, Reliable Computing 7 (3) (2001) 231–246.

[28] M. Mrozek, P. Zgliczyński, Set arithmetic and the enclosing problem in dynamics, Annales Polonici Mathematici 74 (2000).

[29] E. Landau, Handbook on the theory of the distribution of the primes, B.G. Teubner, Leipzig, 1909.

[30] A. Neumaier, Interval Methods for Systems of Equations, Cambridge University Press, Cambridge, UK, 1990. doi:10.1002/zamm.19920721114.

[31] S. Kobayashi, K. Nomizu, Foundations of Differential Geometry, Vol. 1, Interscience Publishers, New York, 1963.

[32] A. Ignazi, N. Delanoue, Manifold decomposition for interval analysis, in: SWIM'23, Angers, 2023.

[33] A. Hatcher, Algebraic Topology, Cambridge University Press, Cambridge, UK, 2001.
URL http://www.math.cornell.edu/~hatcher/AT/ATpage.html

[34] J. W. Alexander, Topological invariants of knots and links, Transactions of the American Mathematical Society 30 (1928) 275–306.

[35] T. Kapela, M. Mrozek, D. Wilczak, P. Zgliczynski, CAPD: dynsys, A flexible C++ toolbox for rigorous numerical analysis of dynamical systems, Communications in Nonlinear Science and Numerical Simulation 101 (2021) 105578. doi:10.1016/j.cnsns.2020.105578.

[36] S. Rohou, B. Desrochers, F. L. Bars, The codac library, Acta Cybernetica 26 (4) (2024) 871–887. doi:10.14232/ACTACYB.302772.

[37] T. Lew, R. Bonalli, L. Janson, M. Pavone, Estimating the convex hull of the image of a set with smooth boundary: Error bounds and applications, Discrete & Computational Geometry (2024) 1–39doi:10.1007/s00454-024-00683-5.
URL https://link.springer.com/10.1007/s00454-024-00683-5

[38] S. Bogomolov, M. Forets, G. Frehse, K. Potomkin, C. Schilling, Juliareach: a toolbox for set-based reachability, in: HSCC 2019, 2009, pp. 39–44.